Helsinki University of Technology
Inorganic Chemistry Publication Series
Espoo 2006 No. 6

ATOMIC LAYER DEPOSITION OF LANTHANIDE OXIDE THIN FILMS

Jani Päiväsaari

Dissertation for the degree of Doctor of Science in Technology to be presented with due permission of the Department of Chemical Technology for public examination and debate in Auditorium V1 at Helsinki University of Technology (Espoo, Finland) on the 19th of May, 2006, at 12 noon.

Helsinki University of Technology
Department of Chemical Technology
Laboratory of Inorganic and Analytical Chemistry

Teknillinen korkeakoulu
Kemian tekniikan osasto
Epäorgaanisen ja analyyttisen kemian laboratorio

Distribution:
Helsinki University of Technology
Laboratory of Inorganic and Analytical Chemistry
P.O. Box 6100
FIN-02150 TKK, FINLAND

ISBN 951-22-8163-5
ISSN 1458-5154

Otamedia Oy
Espoo 2006

ABSTRACT

This thesis describes the processing of thin films of lanthanide (Ln) oxides by atomic layer deposition (ALD) technique. Deposition of all binary lanthanide oxides was studied, excluding terbium oxide and the unstable promethium oxide. In addition, gadolinium oxide-doped cerium dioxide films were grown by combining the respective binary processes developed in this work. Films were characterized by a wide range of analytical techniques for structural, compositional, electrical, and surface properties. As background for the study, some promising application areas for lanthanide and rare earth (RE) oxide thin films are briefly introduced, and the ALD technique is explained. Reported ALD processes for RE oxides are then reviewed.

$Ln(thd)_3$ and ozone were successfully utilized for deposition of most members of the Ln_2O_3 series. The deposited films were nearly stoichiometric Ln_2O_3 with only low concentrations of carbon, hydrogen, and fluorine impurities. Films were also uniform and smooth. Relative permittivity values were in the range of 8.4–11.1.

In addition to $Er(thd)_3$, Er_2O_3 films were also grown with $(CpMe)_3Er$ and $Er(^tBu_2amd)_3$ as metal precursors. All processes resulted in pure and nearly stoichiometric Er_2O_3 films. The growth rate of 1.5 Å/cycle obtained with the $(CpMe)_3Er/H_2O$ process was approximately four and six times the rates measured for erbia films grown by the $Er(^tBu_2amd)_3/O_3$ and $Er(thd)_3/O_3$ processes, respectively.

Cerium dioxide films were successfully deposited with use of $Ce(thd)_4$ or $Ce(thd)_3(phen)$ and ozone as precursors. Gadolinium oxide-doped CeO_2 (CGO) films were then grown by combining the $Ln(thd)_x/O_3$ processes for the respective binary oxides. ALD-grown CGO films were dense and conformal, but the Ce:Gd ratio in the films could not be optimized to the level required in solid oxide fuel cells.

PREFACE

This work was carried out in the Laboratory of Inorganic and Analytical Chemistry, Helsinki University of Technology, between January 2000 and September 2005.

I would like to thank my supervisor Professor Lauri Niinistö for the opportunity to work in his ALD group and for his kind and expert help whenever needed. I am most grateful to my instructor Dr. Matti Putkonen for fruitful research ideas and advice, as well as to the members of the ALD group and especially my co-authors Mr. Jaakko Niinistö, Dr. Charles Dezelah, and Lic.Sci. (Tech.) Anne Kosola for their many contributions. I wish to thank Dr. Minna Nieminen for all the help in finalizing this thesis. I am indebted to the personnel at the Laboratory for practical help.

Special thanks are owed to Dr. Kaupo Kukli for carrying out the electrical measurements and XRR analyses and providing invaluable help in interpreting the results, to Drs. Timo Sajavaara and Kai Arstila for performing the TOF-ERD analyses, to Professors Markku Leskelä (Laboratory of Inorganic Chemistry) and Juhani Keinonen (Accelerator Laboratory) at the University of Helsinki for providing the necessary facilities for these measurements, and to Professor Charles Winter (Wayne State University, Detroit) and Dr. Emmanuel Gourba (Ecole Nationale Supérieure de Chimie de Paris) for fruitful collaboration in the fields of precursor chemistry and solid oxide fuel cells, respectively.

Warmest thanks belong to my beloved wife Minna. Thank you for your unfailing encouragement and support over these many years.

This work was supported by the Foundation of Technology (TES), the Wihuri Foundation, and the Gustav Komppa Fund of the Kordelin Foundation.

Espoo, February 2006

Jani Päiväsaari

LIST OF PUBLICATIONS

The thesis is based on the following publications, which are referred to in the text by Roman numerals I-VII:

I Päiväsaari, J., Putkonen, M., and Niinistö, L., A comparative study on lanthanide oxide thin films grown by atomic layer deposition, *Thin Solid Films* **472** (2005) 275-281.

II Kosola, A., Päiväsaari, J., Putkonen, M., and Niinistö, L., Neodymium oxide and neodymium aluminate thin films by atomic layer deposition, *Thin Solid Films* **479** (2005) 152-159.

III Päiväsaari, J., Putkonen, M., Sajavaara, T., and Niinistö, L., Atomic layer deposition of rare earth oxides: erbium oxide films from β-diketonate and ozone precursors, *J. Alloys Compd.* **374** (2004) 124-128.

IV Päiväsaari, J., Niinistö, J., Arstila, K., Kukli, K., Putkonen, M., and Niinistö, L., High growth rate of erbium oxide thin films in atomic layer deposition from $(CpMe)_3Er$ and water precursors, *Chem. Vap. Deposition* **11** (2005) 415-419.

V Päiväsaari, J., Dezelah, C.L., Back, D., El-Kaderi, H.M., Heeg, M.J., Putkonen, M., Niinistö, L., and Winter, C.H., Synthesis, structure, and properties of volatile lanthanide complexes containing amidinate ligands: application for Er_2O_3 film growth by atomic layer deposition, *J. Mater. Chem.* **15** (2005) 4224-4233.

VI Päiväsaari, J., Putkonen, M., and Niinistö, L., Cerium dioxide buffer layers at low temperature by atomic layer epitaxy, *J. Mater. Chem.* **12** (2002) 1828-1832.

VII Gourba, E., Ringuedé, A., Cassir, M., Päiväsaari, J., Niinistö, J., Putkonen, M., and Niinistö, L., Microstructural and electrical properties of gadolinium doped ceria thin films prepared by atomic layer deposition (ALD), *Electrochem. Soc. Proc.* **2003-7** (2003) 267-274.

THE AUTHOR'S CONTRIBUTION

Publications I and III	The author defined the research plan for the experimental work and performed all practical work except TOF-ERDA and AFM, interpreted the results, and wrote the manuscript.
Publications II	The author participated in the planning of the research, performed some of the experiments, and participated in interpreting the results and writing the manuscript.
Publication IV	The author had a major role in defining the research plan and carried out all practical work, except TOF-ERDA, AFM, and characterization of the electrical properties. The author interpreted the results and wrote a major part of the manuscript.
Publication V	The author defined the research plan for the ALD section of the manuscript, carried out the depositions, and did all thin film analyses except TOF-ERDA and AFM. The author contributed to the writing of the ALD section of the manuscript.
Publication VI	The author defined the research plan with the co-authors and performed all practical work except TOF-ERDA and AFM. The author interpreted the results and wrote the manuscript together with the co-authors.
Publication VII	The author defined the research plan for the ALD part of the manuscript and carried out the depositions and some of the thin film analyses. The author contributed to the writing of the ALD part of the manuscript.

LIST OF ABBREVIATIONS AND ACRONYMS

acac	Acetyl acetonate, 2,4-pentanedionate
AFM	Atomic force microscopy
ALCVD	Atomic layer chemical vapor deposition
ALD	Atomic layer deposition
ALE	Atomic layer epitaxy
ALP	Atomic layer processing
amd	Amidinate
bipy	Bipyridine
CGO	Gadolinia-doped ceria, $Ce_{1-x}Gd_xO_{2-0.5x}$
Cp	Cyclopentadienyl
CVD	Chemical vapor deposition
dmae	Dimethylaminoethoxide
DTA	Differential thermal analysis
EBE	Electron beam evaporation
EDS	Energy dispersive x-ray spectroscopy
EOT	Equivalent oxide thickness
fdh	1,1,1-Trifluoro-5,5-dimethyl-2,4-hexanedionate
FTIR	Fourier transform infrared spectroscopy
IR	Infrared spectroscopy
IT-SOFC	Intermediate temperature solid oxide fuel cell
Ln	Lanthanide element (Ce-Lu)
LSM	Lanthanum strontium manganate, $La_{1-x}Sr_xMnO_3$
mmp	1-Methoxy-2-methyl-2-propanolate
MOSFET	Metal-oxide-semiconductor field effect transistor
Phen	1,10-Phenanthroline
RE	Rare earth (Y, Sc, La, Ce-Lu)
REALD	Radical-enhanced atomic layer deposition
rms	Root mean square
SEM	Scanning electron microscopy
SOFC	Solid oxide fuel cell
tetea	Triethoxy-triethyleneamine
tetraglyme	Tetraethyleneglycol-dimethylether

thd	2,2,6,6-Tetramethyl-3,5-heptanedionate
TG	Thermogravimetry
TOF-ERDA	Time-of-flight elastic recoil detection analysis
tod	2,2,6,6-Tetramethyl-3,5-octanedionate
TMA	Trimethylaluminum, $(CH_3)_3Al$
XRD	X-ray diffraction
XRR	X-ray reflectometry
YSZ	Yttria-stabilized zirconia, Y_2O_3-ZrO_2

CONTENTS

1. INTRODUCTION

The rare earth elements consist of Group 3 metals ($_{21}$Sc, $_{39}$Y, and $_{57}$La) and lanthanides ($_{58}$Ce→$_{71}$Lu). The rare earths (RE) and particularly the lanthanides (Ln) form, chemically and physically, a more or less homogeneous group, the largest in the periodic table (Fig. 1). This is a consequence of the lanthanide contraction, which refers to the gradual decrease in the ionic radius of the elements from lanthanum to lutetium by 17%. Owing to the lanthanide contraction, trivalent yttrium is near in size to the heavier lanthanides and the chemical behaviour is closely similar.[1] Many physical and chemical properties of the rare earth oxides vary only slightly from element to element.[2,3]

The use of rare earths is extensive. Examples of their classical and most recent applications include automotive catalytic converters, glass polishing, petroleum refining catalysts, phosphors, and permanent magnets.[4] RE oxide thin films have already been utilized or they are being considered as potential materials in a variety of applications, particularly in optics and electronics. Some application areas where atomic layer deposited (ALD) RE oxide thin films may find use are presented in Chapter 2. By virtue of their high relative permittivity values (k=12.3–14.8),[5] RE oxides have been considered as candidates for new gate dielectrics in microelectronics.[6-10] Er_2O_3 is being used as a doping material in amplifying optical waveguides, while RE_2O_3-doped CeO_2 films could be employed as oxide ion conducting electrolytes in solid oxide fuel cells (SOFC). The components discussed in Chapter 2 were not actually prepared during this work, but rather ALD processes for many of the relevant materials were designed.

The primary aim of the present work was to develop ALD processes for lanthanide oxides, most of which had not earlier been deposited by ALD technique. ALD can be utilized to produce very thin, but yet dense, uniform, and conformal films.[11,12] As background to the study, the general principle of ALD is described in Section 3.1, and a short literature review on previously reported ALD processes for RE oxides is presented in Section 3.2

The experimental part of this thesis is divided into three parts. The first part deals with the ALD of Ln_2O_3 films using the $Ln(thd)_3/O_3$ process (thd = 2,2,6,6-tetramethyl-3,5-heptanedionate).[I-III] The second part focuses on the deposition of Er_2O_3 films, which are grown from three different metal precursors.[III-V] The suitability of the different precursors for ALD of lanthanide oxides is evaluated on the basis of the properties of the Er_2O_3 films. The results obtained with $(CpMe)_3Er$ (Cp = cyclopentadienyl) are promising for the development of water-based ALD processes for lighter lanthanide oxides. In the third part, the deposition and characteristics of cerium dioxide,[VI] gadolinia-doped CeO_2,[VII,13] and praseodymium oxide thin films[14] are discussed.

Note that the terms ‘rare earth’ and ‘rare earth oxide’ are systematically used in Chapters 2 and 3 even though the focus in Chapters 4 and 5 is on the ALD of lanthanide oxides. Because of the similarities in the properties of the rare earth elements, the application areas and precursor chemistry of lanthanide oxides are very much the same as those for oxides of Group 3 metals and thus they can be discussed together under the broader term rare earth oxides.

1	2	3	4	5	6	7	8	9	10	11	12	13	14	15	16	17	18
1 H																	2 He
3 Li	4 Be											5 B	6 C	7 N	8 O	9 F	10 Ne
11 Na	12 Mg											13 Al	14 Si	15 P	16 S	17 Cl	18 Ar
19 K	20 Ca	21 Sc	22 Ti	23 V	24 Cr	25 Mn	26 Fe	27 Co	28 Ni	29 Cu	30 Zn	31 Ga	32 Ge	33 As	34 Se	35 Br	36 Kr
37 Rb	38 Sr	39 Y	40 Zr	41 Nb	42 Mo	43 Tc	44 Ru	45 Rh	46 Pd	47 Ag	48 Cd	49 In	50 Sn	51 Sb	52 Te	53 I	54 Xe
55 Cs	56 Ba	57 La*	72 Hf	73 Ta	74 W	75 Re	76 Os	77 Ir	78 Pt	79 Au	80 Hg	81 Tl	82 Pb	83 Bi	84 Po	85 At	86 Rn
87 Fr	88 Ra	89 Ac**	104 Rf	105 Db	106 Sg	107 Bh	108 Hs	109 Mt	110 Ds	111 Rg							

Lanthanides*	58 Ce	59 Pr	60 Nd	61 Pm	62 Sm	63 Eu	64 Gd	65 Tb	66 Dy	67 Ho	68 Er	69 Tm	70 Yb	71 Lu
Actinides**	90 Th	91 Pa	92 U	93 Np	94 Pu	95 Am	96 Cm	97 Bk	98 Cf	99 Es	100 Fm	101 Md	102 No	103 Lr

Fig. 1 In the periodic table lanthanides (elements 58–71 from Ce-Lu) are usually drawn as a separate group below the main table. Lanthanides together with the group 3 metals (Sc, Y, and La) are known as rare earth elements.

2. POTENTIAL APPLICATIONS FOR RARE EARTH OXIDE FILMS

This chapter discusses three promising application areas for rare earth oxide thin films and indicates the suitability of the ALD technique to the processing of these films. ALD processes for many of the relevant materials will be introduced in Chapters 3 and 4.

2.1. Metal-oxide-semiconductor field effect transistors

The scaling down of metal-oxide-semiconductor field effect transistors (MOSFET, Fig. 2) has been a continuous trend in microelectronics, the number of transistors per chip being doubled every one and a half or two years.[10] This trend was predicted as long ago as 1965 by Gordon Moore and is known as Moore's Law.[15] The motivation for downscaling is manufacturing of faster transistors with lower power consumption.[16] The dimensions of MOSFETs have now reached the level where the current silicon-based gate materials, namely SiO_2 gate dielectric and poly-Si gate electrode, will have to be replaced with other materials if miniaturization is to continue.[10,17]

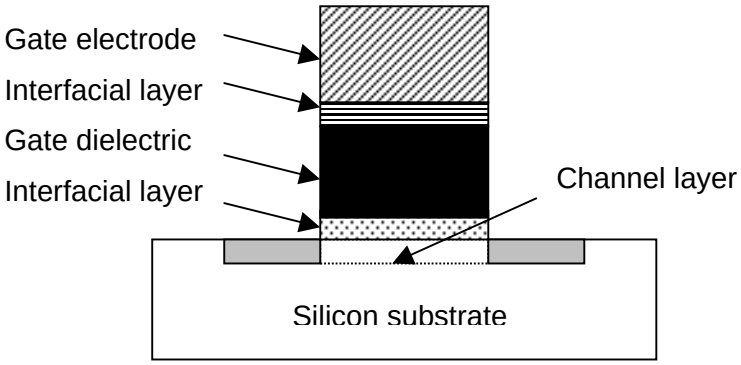

Fig. 2 A schematic presentation of the gate stack in a MOSFET.

Transistor speed is dependent on drive current, $I_{D,sat}$, which can be written

$$I_{D,sat} = \frac{W}{L}\mu C_{inv}\frac{V_{D,sat}^2}{2}, \qquad (1)$$

where W is the channel width, L is the channel length, μ is the charge carrier mobility in the channel, C_{inv} is the capacitance density of the gate dielectric when the channel is in the inverted state, and $V_{D,sat}$ is the potential applied to the drain of the transistor.[16,17] Because the maximum value of $V_{D,sat}$ is limited due to reliability

constraints, the channel length L has to be reduced and/or the capacitance density of the gate dielectric has to be increased in order to enhance the drive current, $I_{D,sat}$, and the transistor speed. The capacitance density of the dielectric can also be written

$$C_{inv} = \frac{C}{A} = \frac{k\varepsilon_0}{t} \ , \qquad (2)$$

where C is the capacitance of the gate dielectric, A is the area of the capacitor, k is the dielectric constant of the gate material, ε_0 is the permittivity of free space (8.85×10^{-3} fF/μm), and t is the thickness of the dielectric layer.[17] Thus, the capacitance density can be increased by applying a thinner gate dielectric layer or using a material with higher dielectric constant.

The currently used MOSFET dielectric material, SiO_2, can be scaled down only to a thickness of approximately 10–15 Å.[17,18] Leakage current through a thinner SiO_2 layer would be too high, and operating voltage would result in catastrophic breakdown.[19] If a material with a higher dielectric constant were used, the charge storing capacity of the capacitor could be increased without using a too thin dielectric layer.[16,17]

A high permittivity (high-k) gate oxide capacitor is usually compared with a conventional SiO_2 capacitor in terms of equivalent oxide thickness, t_{eq} (EOT), where EOT is the theoretical thickness of a SiO_2 layer that would have the same charge density as the high-k dielectric. The EOT value of the high-k MOSFET is required to be less than 1 nm.[10] It should be noted that if the gate dielectric reacts with the substrate, an interfacial SiO_2 layer is typically formed. The relative permittivity of SiO_2 is low (k=3.9) and thus it reduces the capacitance C_{TOT} of the gate stack, since

$$\frac{1}{C_{TOT}} = \frac{1}{C_1} + \frac{1}{C_2} , \qquad (3)$$

where C_1 and C_2 represent the capacitances of the interfacial and high-k layers, respectively. At the same time the EOT of the gate stack also increases. EOT of the stack is

$$t_{eq} = t_{SiO_2} + \frac{k_{SiO_2} \times t_{high-k}}{k_{high-k}} . \qquad (4)$$

At the moment, it appears that the next generation of gate dielectrics will be based on hafnium oxides and silicates, but in the rather near future these Hf-based materials may have to be replaced as well.[10] Rare earth oxides are among the candidates for the next generation of gate dielectrics. They are thermodynamically stable in contact with silicon,[20] and their relative permittivity values are large enough, being in the range of 12.3–14.8 for bulk oxides[5] but a value as high as 27 has been reported for a La_2O_3 thin film.[21] The band gap and conduction band offset values of RE oxides also meet the requirements for gate dielectrics, being *ca.* 4–6 eV and >2 eV, respectively.[8-10,22] There are many other critical factors influencing the choice of the next gate dielectric material. In the case of RE oxides, issues such as interface quality, morphology, compatibility with other gate materials, film processing compatibility, and reliability call for further research.[10,17] The scaling down of MOSFETs places demands on the thin film deposition technique as well, and ALD may well be the method-of-choice for the deposition of gate dielectrics in the near future[10,22,23] since it can be utilized to deposit very thin and yet conformal films even into deep trenches.[11,12]

2.2. Optical waveguides

Optical waveguides are employed to carry optical signals along a desired path. Waveguides can be either planar or, more typically, fiber-like. Planar waveguides consist of an optically suitable thin film material prepared on a substrate, whereas in fibers the optical signal propagates in the core material of the fiber. In both types of waveguide, the transmission medium of the optical signal is surrounded by a cladding, which has a lower refractive index than the transmission material. The optical signal is transmitted farther in the waveguide if the angle at the core-cladding interface is less than the critical angle for total internal reflection (Fig. 3). The typical transmission medium for light is glass, consisting of SiO_2, with possible additives that modify the refractive index.[24,25]

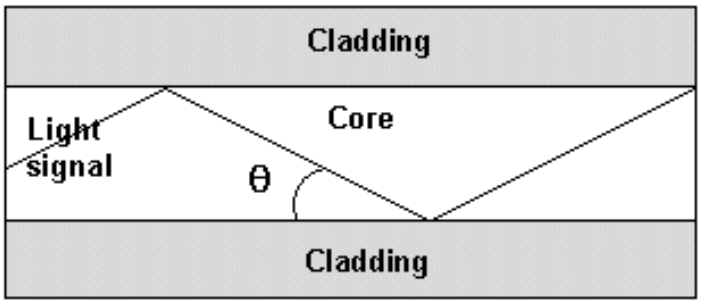

Fig. 3 Light is guided along the transmission medium by total internal reflection. θ is the incidence angle of light at the core-cladding interface.

The intensity of the optical signal is reduced along the waveguide due to absorption and scattering.[24,25] The transmission loss in SiO_2-containing fibers is lowest at approximately 1.50 μm, which is therefore used as a standard wavelength in optical telecommunication systems.[24-26] The attenuation (or transmission loss) of the optical signal has to be compensated by employing optical amplifiers. In most cases, the amplifying materials contain rare earth ions as dopants, and erbium-doped materials are of great interest.[26] The transition energy between the first excited state and the ground state of Er^{3+} ions corresponds to a wavelength of 1.53 μm. Therefore, if Er^{3+} ions are excited externally, for example by a laser, the transition energy can be employed to provide gain in the optical signal. Use of ytterbium ions as sensitizers in Er-doped amplifiers enables the use of shorter wavelength lasers.[26] Solubility of rare earth ions in pure silica is very low, however, and clusters of RE ions will quickly start to form reducing the number of optically active RE ions.[27] However, if silica is first doped with Al_2O_3 the clustering is eliminated and doping concentrations for RE ions can be much higher.[27] In planar waveguides, the transmission medium can be simply aluminum oxide doped with RE ions.[26,28,29] The concentration of Er^{3+} ions has to be carefully controlled in order to achieve optimum amplification. In planar Er-doped Al_2O_3 waveguides the optimal Er concentration is approximately 3×10^{20} ions/cm^3 (~0.3 at.-%).[26,28]

With ALD the level of doping can be controlled in a straightforward manner, even on large deposition areas, and ALD should therefore be a highly suitable method for preparing planar waveguides for integrated optical circuits. In fact, Solehmainen *et al.*[29] have already demonstrated the fabrication of planar Er-doped alumina waveguides by ALD, but their process needs further development to achieve a more

homogeneous distribution of Er-atoms. From the above, it is clear that the development of new ALD processes for Er_2O_3 and other rare earth oxides is of considerable importance.

2.3. Solid oxide fuel cells

Fuel cells convert the chemical energy of fuels such as H_2, CO, hydrocarbons, and alcohols to electrical energy. The operating principle of solid oxide fuel cells (SOFC, Fig. 4) is the following: (1) The fuel reacts at the anode with oxide ions that have travelled through the solid electrolyte, and (2) the liberated electrons travel through an external circuit to the cathode, where (3) oxygen is catalytically reduced to oxide ions.

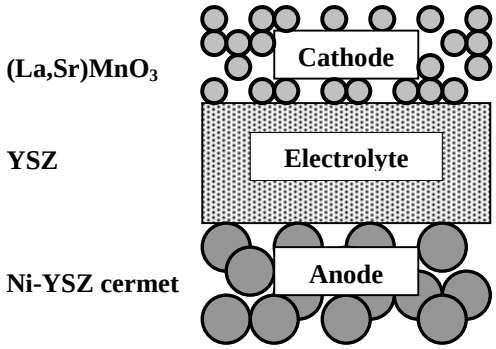

Fig. 4 Schematic presentation of a typical SOFC comprising $(La,Sr)MnO_3$ and Ni-YSZ electrodes and YSZ electrolyte.

The most commonly employed electrolyte material today is yttria-stabilized zirconia (YSZ), while $(La,Sr)MnO_3$ (LSM) and Ni-YSZ cermet have been used as electrodes. The operating temperature of state-of-the-art SOFCs having the Ni-YSZ/YSZ/LSM structure is above 950 °C. Lowering of the operating temperature to 500–750 °C would lengthen the lifetime of SOFCs and allow the use of less expensive interconnecting materials. However, there are many thermally activated processes in SOFCs, such as oxide ion conductivity, chemical reactions at electrodes, and internal reforming of fuel, and adjustment of the operating temperature requires a careful balancing of the benefits and disadvantages.[30] Intermediate temperature SOFCs (IT-

SOFC) operated at 500–750 °C can be realized if the decrease in the ionic conductivity of the electrolyte is compensated by selecting a more conductive electrolyte material or using a thinner electrolyte layer.[30]

Potential new electrolyte materials for IT-SOFCs include CeO_2,[31-34] ZrO_2,[35] ThO_2[36] and Bi_2O_3,[37] typically doped with rare earth oxides. RE_2O_3-CeO_2 solid solutions with fluorite structure are a well-known group of oxide ion conductors[31,38] and are considered as the most promising alternative materials for IT-SOFCs despite their instability under reducing atmospheres.[31,39] Special attention has been paid to gadolinia-doped ceria (CGO) or $Ce_{1-x}Gd_xO_{2-0.5x}$, which appears to have the highest conductivity among ceria-based electrolytes.[31,33] As the dopant concentration in the CGO system is increased, the conductivity passes through a maximum.[40] The maximum in ionic conductivity is obtained when *ca.* 10 at.-% of Ce is substituted by Gd, *i.e.* $Ce_{0.9}Gd_{0.1}O_{1.95}$, but the exact position of the maximum is also dependent on the temperature.[40] Other interesting ceria-based systems are samaria-doped and yttria-doped ceria, which exhibit about the same conducting properties as the CGO electrolyte.[31,41,42]

The thickness of the electrolyte layer in thin film IT-SOFCs is typically 5–10 μm, which is very much less than the 200 μm used in conventional SOFC devices. This means that even less conductive electrolyte materials, such as YSZ, can be employed in thin film IT-SOFCs.[43] The processing of the electrolyte and the electrodes by thin film deposition techniques also improves properties of the interface.[44] Although YSZ thin film electrolytes have been the prime research target, ceria-based thin film electrolytes and interlayers have been widely studied as well. Ceria-based interlayers between the actual electrolyte and the electrodes have been reported to enhance the cell performance because they significantly reduce polarization losses.[45] Previously, CGO electrolyte films have been processed by *e.g.* spray pyrolysis,[46] aerosol-assisted metal-organic CVD,[47] and tape casting.[48] Furthermore, screen-printing[49] and sputtering[45] methods have been utilized to deposit CGO and yttria-doped CeO_2 interlayers, respectively. In this work, ALD was applied for the preparation of CGO thin film electrolytes.[VII,13]

3. ATOMIC LAYER DEPOSITION OF RARE EARTH OXIDES

The basic principle of the ALD technique is now introduced, and the ALD processes for binary RE oxides as well as for RE-containing multicomponent oxide thin films are reviewed. In Section 3.2, ALD processes for binary oxides are discussed according to the precursor employed and those for multicomponent RE-containing oxide films according to the structure of the film. Characteristics of the deposited films are briefly discussed. All the processes are summarized in Tables 1 (p. 28) and 2 (p. 33). The ALD processes that were developed in this work are presented in a more detailed way in Chapters 4 and 5.

3.1. Principle of atomic layer deposition

Atomic layer deposition (ALD) is a gas-phase thin film deposition technique, which can be considered as an advanced version of chemical vapor deposition (CVD). It has also been referred to as atomic layer epitaxy (ALE), atomic layer chemical vapor deposition (ALCVD), atomic layer growth (ALG), atomic layer processing (ALP), and layer-by-layer deposition.[11,12] ALD is particularly suitable for the deposition of binary films such as oxides, nitrides, and sulfides, but also numerous more complex films have successfully been processed.[11,12,50-52] A schematic diagram of the ALD reactor used in this work is presented in Fig. 5.

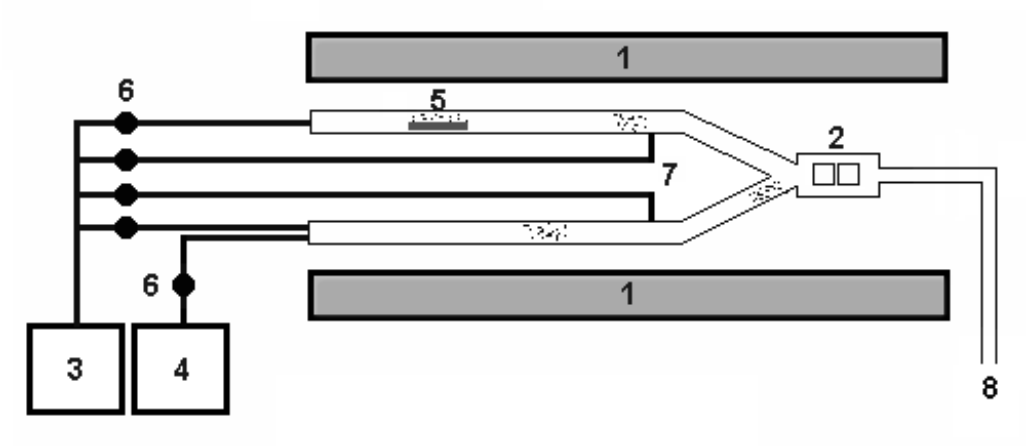

Fig. 5 A schematic diagram of a satellite-type ALD reactor used in this work. (1) Heating elements, (2) reaction chamber and substrates, (3) N_2 generator, (4) external source for gaseous precursors, such as O_3, (5) source boat for RE precursor, (6) pulsing valves, (7) inlets for inert gas purging, and (8) outlet to the vacuum pump.

In ALD, precursors are alternately introduced to the reaction chamber, where they saturatively react with the substrate surface. Precursors are separated from each other by an inert gas purge, which removes the excess of precursor molecules and volatile reaction by-products from the reaction chamber, thus preventing undesired gas-phase reactions. Pulsing and purging times are normally 1-3 s, depending on the precursors applied.

A growth cycle in ALD of binary materials typically consists of four steps, as illustrated in Fig. 6 for an ALD process employing REL_3 (L = ligand) and water as precursors. In the ALD processes using water as the oxygen source, the growth of oxide film occurs *via* hydroxyl groups bonded to the surface.[11,53] For example, when the growth reactions of ZrO_2 from $Cp_2Zr(CH_3)_2$ and deuterated water were recently studied,[54] $Cp_2Zr(CH_3)_2$ was proposed to react with the OD-groups on the surface releasing CH_3D and CpD as by-products. The remaining Cp groups were released during the subsequent D_2O pulse and the surface was reverted to OD-terminated. Among the RE precursors cyclopentadienyl, alkoxide, and amidinato complexes have been demonstrated to react with water (see Table 1, p. 28), but *in situ* studies of these processes have not been reported. The growth reactions in the ozone-based ALD processes have rarely been studied. Liu *et al.*[55] and Kim *et al.*[56] studied the $Hf[(N(CH_3)(CH_2CH_3)]_4/O_3$ and $Zn(CH_2CH_3)_2/O_3$ processes, respectively, while Puurunen[57] has proposed a theoretical model for the Y_2O_3 growth from $Y(thd)_3$ and O_3. Ozone is probably such a strong oxidizer that it burns off the ligands to water and carbon dioxide.[56,57] The water may subsequently react with the surface species and generate –OH groups for the next ALD cycle.

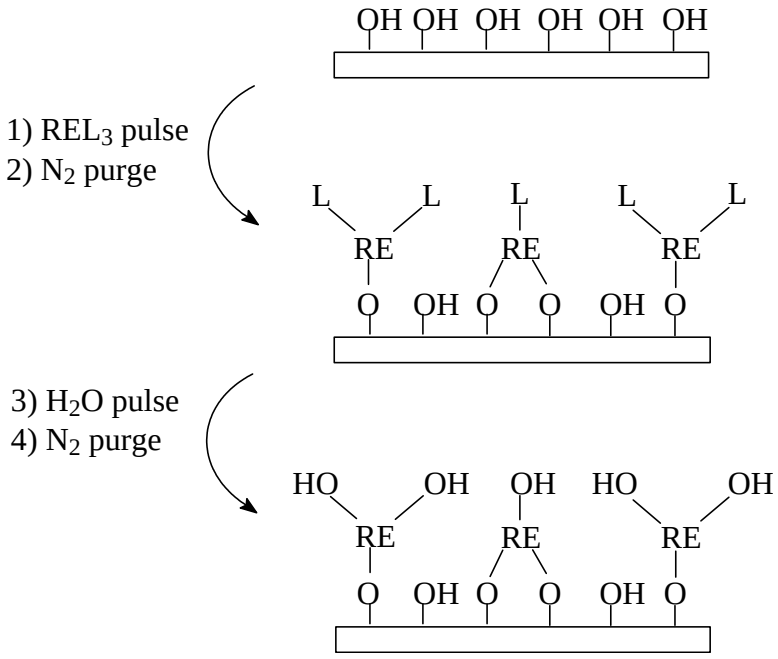

Fig. 6 An ALD cycle consists of two precursor doses (Steps 1 and 3), separated by inert gas pulses (Steps 2 and 4), as schematically illustrated for RE oxide deposition from REL_3 (L = ligand, *e.g.* cyclopentadienyl or alkoxide group) and H_2O precursors. The volatile surface reaction by-products, such as CpH or ROH, are purged away with inert gas.

When the deposition conditions in ALD are optimal, the film growth proceeds through saturative, self-limiting surface reactions. The temperature range where this ALD-type self-terminating growth takes place often leading to a constant growth rate as well, is known as the ALD window.[12,50,51,58] Ideally, one ALD cycle produces one monolayer of material, but owing to steric hindrances or lack of reactive surface sites, the growth rate per cycle tends to be considerably lower.[50] This is also evident in Fig. 6, where for steric reasons the large REL_3 molecules are unable to react with all -OH groups bound to the surface. The film thickness increment per cycle, *i.e.* the *g*rowth rate, is nevertheless constant, and the thickness of the thin film can be controlled simply through the number of deposition cycles. Besides the easy and accurate control of thickness, the self-limiting growth mechanism leads to excellent uniformity and conformality, and provides excellent trench filling capability.[59]

ALD precursors have to meet several requirements.[11,50] First of all, they must be sufficiently volatile for efficient gas-phase transportation but yet thermally stable in order to prevent uncontrolled decomposition reactions. Gas-phase reactions between

precursors are avoided in ALD because precursors are introduced to the reaction chamber alternately with an inert gas purge. Precursors that are highly reactive toward each other are even favored in ALD, because reactions are then complete, the resulting thin films are of high purity, and pulsing times can be shorter. Purity, low price, low toxicity, ease of handling, and easy synthesis are desirable, but not essential properties of the precursors.[11]

3.2. Literature review on ALD of rare earth oxide thin films

Thin films containing rare earth oxides have been deposited by both physical and chemical thin film deposition techniques. Among these are electron beam evaporation (EBE),[60-65] sputtering,[45,66] spray pyrolysis,[46,67] and CVD.[47,68-87] The number of ALD processes is still rather limited, but the ALD of RE oxide thin films has recently been gaining interest especially in the context of high-k research (see Section 2.1).[6-10] At the same time, the number of scientific papers on ALD of RE oxides has been increasing. The following review of the ALD of RE oxides is based on a recently published review,[88] which is supplemented and updated.

3.2.1. ALD of binary RE oxides

ALD processes have successfully been developed for almost all binary rare earth oxides, the sole exception being terbium oxide and the unstable promethium (see Table 1, p. 28). As yet, there are only a limited number of ALD precursors for rare earth oxides. These precursors can be divided into five groups: (i) β-diketonates, (ii) alkoxides, (iii) organometallics, (iv) amides, and (v) amidinates (Fig. 7). The majority of the processes reported so far are based on β-diketonates,[I-III,VI,VII,89-98] and β-diketonates were also the most intensively studied precursors in this work. Alkoxides are another type of oxygen-coordinated precursor, but although these are commonly used in CVD, there is only one report of an alkoxide precursor being employed in the ALD of RE oxides.[99] Most recently, organometallic cyclopentadienyl-based precursors[IV,89,95,100,101] as well as nitrogen-coordinated amides[102-108] and amidinates[V,109-113] have been studied as RE precursors. The choice of the oxygen source depends on the precursor and its reactivity, and ozone, oxygen plasma, and water have all been used in the ALD of RE oxides.

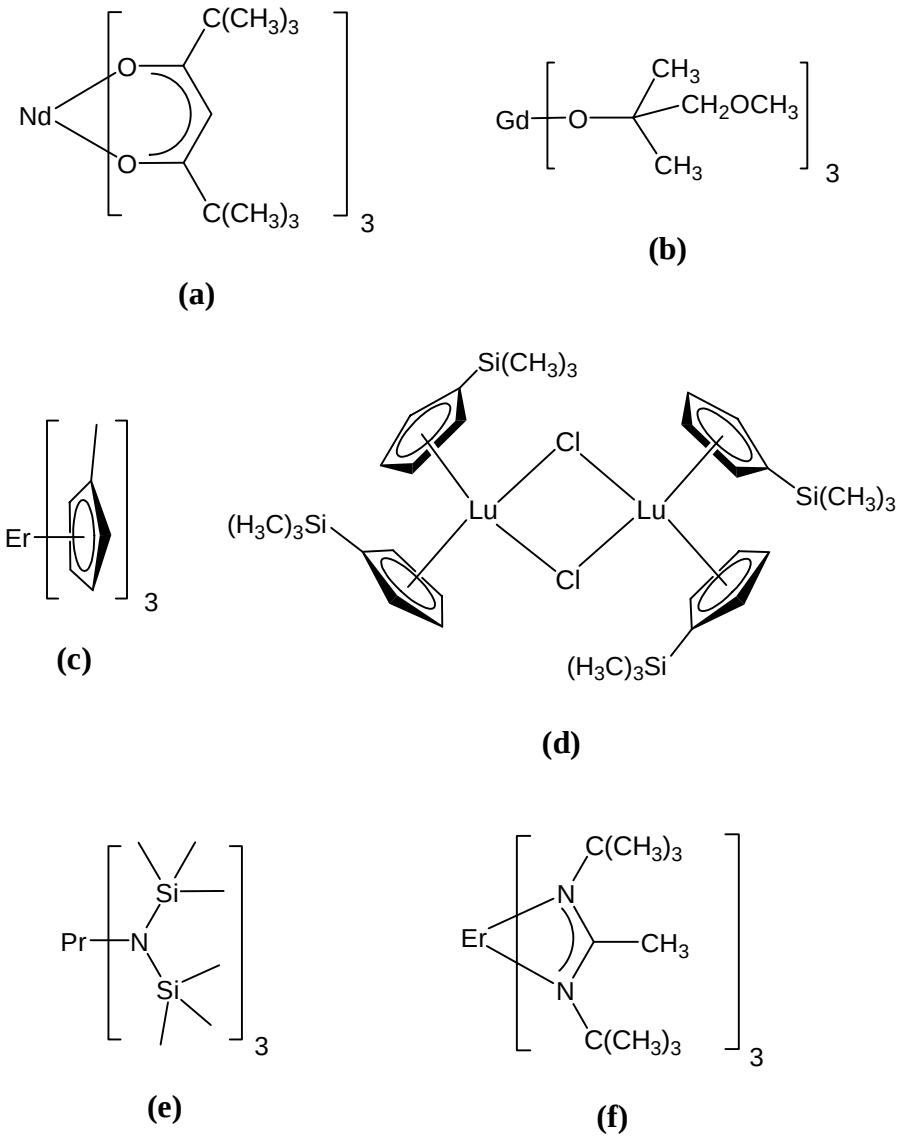

Fig. 7 Examples of metal precursors used in ALD of RE oxide thin films. (a) β-diketonate: $Nd(thd)_3$ (thd = 2,2,6,6-tetramethyl-3,5-heptanedionate);[I,II] (b) alkoxide: $Gd(mmp)_3$ (mmp = 1-methoxy-2-methyl-2-propanolate);[99] (c) cyclopentadienyl-containing complexes: $(CpMe)_3Er$ (Cp = cyclopentadienyl),[IV] (d) $\{[Cp(SiMe_3)]_2LuCl\}_2$;[101] (e) alkyl silylamide: $Pr[N(SiMe_3)_2]_3$;[106] and (f) amidinate: $Er(^tBu_2amd)_3$ (amd = amidinate).[V]

β-diketonates. Although rare earths form few volatile compounds, the volatility of certain rare earth β-diketonates with bulky substituents has been known since the 1960s.[114] The volatility of these complexes has been exploited in CVD and ALD, where they have been widely used as precursors. Many types of RE β-diketonates have been employed in CVD, but most typically complexes of 2,2,6,6-tetramethyl-

3,5-heptanedione, H(thd). In fact, all RE oxides have been deposited from $RE(thd)_x$ precursors by conventional CVD,[68-75] plasma-enhanced CVD (PECVD),[76] or liquid injection CVD.[77,78] Even bulkier ligands such as 2,2,6,6-tetramethyl-3,5-octanedione, H(tod) have occasionally been used.[72] Fluorination of ligands enhances the volatility,[114,115] and fluorinated complexes like $Ce(fdh)_4$ (fdh = 1,1,1-trifluoro-5,5-dimethyl-2,4-hexanedionate) have been exploited as well.[69] In addition, different adducts of RE β-diketonate complexes have been applied, including $La(thd)_3(tetea)$,[79] $Ce(thd)_3(phen)$,[69] $Gd(thd)_3(tetraglyme)$,[80] and $Ln(acac)_3(phen)$[81,82] (tetea = triethoxy-triethyleneamine; phen = 1,10-phenanthroline; tetraglyme = tetraethyleneglycol-dimethylether; acac = acetylacetonate).

Among the many volatile β-diketonates, only thd-based complexes have been utilized as precursors in ALD. These are also the most frequently used rare earth source in ALD.[I-III,VI,VII,89-98] The major part of the $RE(thd)_x$-based ALD processes were developed in the course of the present work and are discussed in a more detailed way in Chapters 4 and 5. All thd-based processes have certain general features, however, which are appropriately mentioned here. $RE(thd)_x$ complexes are volatile, thermally stable solids,[116-118] which are easy to synthesize.[119] They are also easy to handle and store, being relatively stable in contact with air. The optimized deposition temperature range (ALD window) is wide, typically extending from about 250 to 350 °C. β-Diketonate-based processes also have some drawbacks. First, thd-complexes do not react with water but require a stronger oxidizer such as ozone. This could be a problem in the high-k applications. Secondly, the growth rates obtained in $RE(thd)_x/O_3$ processes are rather low, typically on the order of 0.2–0.45 Å/cycle.

Neutral N-donor adducts of $Y(thd)_3$ and $Ce(thd)_3$ complexes have been used as precursors in ALD of Y_2O_3 and CeO_2.[VI,90] Comparison of $Y(thd)_3/O_3$, $Y(thd)_3(phen)/O_3$, and $Y(thd)_3(bipy)/O_3$ (bipy = bipyridine) processes and of $Ce(thd)_4/O_3$ and $Ce(thd)_3(phen)/O_3$ processes failed to reveal any distinct advantages of adducts in the deposition of oxide films. The growth rate, the deposition temperature range, and impurity levels of carbon and hydrogen were similar for adduct and non-adduct precursors in both cases. Moreover, Y_2O_3 films deposited from $Y(thd)_3(phen)$ and $Y(thd)_3(bipy)$ were observed to contain a small amount (0.1–0.3 at.-%) of nitrogen.[90] Adducts such as $Ce(thd)_3(phen)$ may nevertheless be

useful when trivalent cerium ions are needed (*e.g.* in ALD of electroluminescent SrS:Ce thin films) because adducts help to coordinatively saturate the Ce^{3+} ion, thereby stabilizing the otherwise unstable oxidation state of cerium.[120]

Thd precursors have also been used in radical-enhanced ALD (REALD), but so far the results have not been promising. In this technique, reactive oxygen radicals from oxygen plasma are reacted with $Er(thd)_3$ or $Y(thd)_3$ to deposit the respective oxide thin films.[96-98] In the case of both Er_2O_3 and Y_2O_3 films, the ALD window was at 200–300 °C. The obtained growth rate was 0.3–0.5 Å/cycle depending on the precursor pulsing times,[96-98] but the carbon impurity level was high being approximately 26 at.-%. Furthermore, the pulse times needed in the REALD process for Er_2O_3 were ~5–10 min or hundreds of times longer than in a typical flow-type ALD reactor. The reason for such long pulsing times was not discussed in these reports, but they are related to the reactor design. The REALD reactor had a larger reaction chamber, which was equipped with *in situ* instruments, and it was operated under ultra high vacuum conditions.[96-98]

Alkoxides. In general, alkoxides are widely used in CVD,[121] but only recently has the CVD of rare earth oxides from alkoxide precursors been reported.[83-87] The problem has been the tendency of the simple RE alkoxides to form oligomers, which are of low volatility.[121] Recently LaO_x, PrO_x, Nd_2O_3, and GdO_x were grown by liquid injection CVD with $Ln(mmp)_3$ (mmp = 1-methoxy-2-methyl-2-propanolate) alkoxide complex as the metal precursor.[83-87] The same precursors have also been applied in a modified ALD technique, called liquid injection ALD, for the processing of PrO_x and Gd_2O_3 films.[99] In this technique, the precursor solution is injected into a vaporizer and further directed into the reactor chamber, while oxidizer, such as water vapor, is directly pulsed into the reactor chamber. Between the precursor pulses the chamber is purged with inert gas. In ALD of PrO_x and Gd_2O_3 films,[99] the alkoxide precursor $Ln(mmp)_3$ was dissolved in toluene, and tetraglyme, $CH_3(OCH_2CH_2O)_4CH_3$, was added to inhibit condensation and bridging reactions of the precursor molecules. The growth rate was nevertheless observed to increase with increasing precursor dose, indicating a lack of self-limiting behavior and thus the absence of ALD-type growth.[99] The thermal decomposition of the $Ln(mmp)_3$ precursors might explain this observation, but alkoxides may also decompose by β-hydride elimination pathway as

recently demonstrated by Matero *et al.*[122] β-Hydride elimination of the $Ln(mmp)_3$ precursors would generate Ln-OH surface species, thus preventing an ALD-type growth.

Cyclopentadienyl complexes. Organometallic cyclopentadienyl (Cp) complexes contain at least one direct bond between the central metal ion and the $C_5H_5^-$ ligand.[123] Cp compounds have been used as precursors in ALD since the early 1990s.[124] Many Cp complexes are considered as attractive precursors because they are volatile and thermally stable, but yet highly reactive. Their ready reaction with water makes them suitable for the ALD of oxide thin films. Next to thd compounds, cyclopentadienyl-type complexes have been the most frequently studied precursor group in the ALD of RE oxides (see Table 1). So far, however, Cp-based processes have only been developed for the smaller RE oxides, *viz.* Sc_2O_3,[89] Y_2O_3,[95] Gd_2O_3,[100] Er_2O_3,[IV] and Lu_2O_3;[101] no ALD processes are reported for larger RE oxides (RE = La-Eu). Preliminary studies with $(CpMe)_3Ce$ and Cp_3Pr were performed in this work,[14] but controlled growth of the respective oxides was not achieved. Previously, $(CpMe)_3Ce$ was successfully used as a dopant source in ALD of SrS:Ce electroluminescent thin films.[125]

Growth rates were high in ALD of Sc_2O_3,[89] Y_2O_3,[100] Gd_2O_3,[95] and Er_2O_3 [IV] thin films from Cp_3Sc, Cp_3Y or $(CpMe)_3Y$, $(CpMe)_3Gd$, and $(CpMe)_3Er$, respectively – as much as six times as high as the rates obtained in the corresponding thd processes.[I,III,89,95] The $(CpMe)_3Gd/H_2O$ process was not entirely self-limiting due to the partial decomposition of $(CpMe)_3Gd$,[95] but the corresponding Y and Er complexes, $(CpMe)_3Y$ and $(CpMe)_3Er$, as well as Cp_3Sc were thermally stable in the optimized deposition temperature range and were successfully applied in ALD of the respective oxides.[IV,89,100] Every process yielded highly pure films with only low concentrations of carbon and hydrogen. The $(CpMe)_3Er/H_2O$ process, as well as the $(CpMe)_3Ce/H_2O$ and Cp_3Pr/H_2O processes, were studied in this work and are discussed more thoroughly in Sections 4.2, 4.3, and 5.2–5.4.

Lu_2O_3 thin films have been deposited from a silylated dimeric Cp compound, $\{[Cp(SiMe_3)]_2LuCl\}_2$, and water as the precursors.[101] The films were deposited at 360 °C, although the precursor was reported to partially decompose above 250 °C.

An ALD-type self-limiting growth mechanism was probably not achieved therefore, but the variation in thickness of the films as a function of precursor pulse length was not reported. At 7 at.-%, as-deposited films also had a high level of chlorine impurity. Even though it was probably not a true ALD process, the deposited Lu_2O_3 films had relatively good electrical properties (k = 10–12).

Amides. There are only a few examples of nitrogen-coordinated complexes, such as metal amidinates or amides, being used as precursors in the ALD of RE oxides. Simple rare earth alkylamides, $RE(NR_2)_3$, are unstable and not suitable as CVD or ALD precursors.[106] However, RE alkyl silylamides are volatile, thermally relatively stable, and yet reactive toward water.[126] RE silylamides were first employed in ALD for the processing of electroluminescent SrS:Ce thin films, when $Ce[N(SiMe_3)_2]_3$ was used as the dopant source.[127] $RE[N(SiMe_3)_2]_3$ complexes have recently been utilized in ALD of LaO_x, PrO_x, and GdO_x films,[102-108] although in CVD these precursors result in the formation of RE silicates.[85,128]

It appears likely that owing to decomposition of the silylamide precursor, $RE[N(SiMe_3)_2]_3/H_2O$ (RE = La, Pr, or Gd) processes cannot be employed in ALD to produce RE_2O_3 films of sufficient purity. LaO_x films grown from $La[N(SiMe_3)_2]_3$ have been reported to contain relatively high impurity concentrations, particularly the silicon contamination being large (4–10 at.-%).[105,106,108] In addition, Kukli *et al.*[108] reported a very high hydrogen concentration of 39 at.-% in their LaO_x films, but it was attributed to water which had probably diffused into the films from the ambient during storage. The growth rates reported for the $La[N(SiMe_3)_2]_3/H_2O$ process varied noticeably. Whereas Triyoso *et al.*[105] obtained a growth rate of approximately 0.3–0.5 Å/cycle at 250 °C, He *et al.*[103] obtained a rate almost one decade higher, 4.3 Å/cycle, under similar deposition conditions. Although Triyoso *et al.*[105] reported surface saturative growth of uniform La_2O_3 films at deposition temperatures of 225–275 °C, the reported impurities and the detailed study by Kukli *et al.*[108] suggest that the $La[N(SiMe_3)_2]_3$ precursor decomposes during the deposition and the process is therefore not entirely self-limiting.

$RE[N(SiMe_3)_2]_3/H_2O$ process has also been employed in ALD of PrO_x and GdO_x thin films.[106,107] Owing to the decomposition of the silylamide precursor, truly self-

limiting ALD-type growth could not be achieved in either case, however. As-deposited PrO_x films were reported to contain high hydrogen (12–36 at.-%) and silicon (4–10 at.-%) impurity concentrations, while annealed "PrO_x" films deposited were actually characterized as Pr-silicates, $Pr_{9.33}(SiO_4)_6O_2$.[106] The impurities in the GdO_x films were not reported. The growth rates obtained in the PrO_x and GdO_x processes depended strongly on the precursor pulse length and on the deposition temperature. In the PrO_x process, growth rates of 1.1–3.0 Å/cycle and 0.15–0.34 Å/cycle were obtained at 200 °C and 300 °C, respectively. The effective permittivities of as-grown films were relatively good, however, being 14–16 for PrO_x and 10 for GdO_x.[106,107]

Amidinates. The synthesis of a number of RE complexes containing amidinate ligands has been reported.[V,110,111] *N*,*N*'-Dialkyl-2-alkyl amidinates, or RE(RNCR'NR'')$_3$, are volatile and thermally stable.[110,111] The large alkyl groups hinder oligomerization thus enhancing volatility, while the bidentate chelate effect increases the thermal stability.[111] RE amidinates have also been studied as ALD precursors.[V,109-113] Sc_2O_3, Y_2O_3, and La_2O_3 thin films have reportedly been grown using an amidinato complex with isopropyl side groups,[109-111] RE[^{i}PrNC(CH$_3$)N^{i}Pr]$_3$ or RE(^{i}Pr$_2$amd)$_3$ (amd = amidinate), whereas in this work an erbium complex with larger tert-butyl side groups, Er(^{t}Bu$_2$amd)$_3$, was used in the ALD of Er_2O_3 films.[V] Sc(^{i}Pr$_2$amd)$_3$, Y(^{i}Pr$_2$amd)$_3$, and La(^{i}Pr$_2$amd)$_3$ precursors were reported to be reactive toward water, but ozone, as a more reactive oxidizer, was needed for the Er(^{t}Bu$_2$amd)$_3$ complex. The growth rates obtained with the Sc(^{i}Pr$_2$amd)$_3$/H_2O, Y(^{i}Pr$_2$amd)$_3$/H_2O, and La(^{i}Pr$_2$amd)$_3$/H_2O processes at optimized deposition temperatures were 0.7, 0.8, and 0.9 Å/cycle respectively,[109-111] but otherwise very few details were given on the growth behavior, film composition, or properties of the Sc_2O_3 and La_2O_3. Y_2O_3 films were reported to have low impurity concentrations and relatively good dielectric properties ($k \approx 11–12$), but they contained an excess of oxygen (O/Y ratio = 1.7–2.0).[109] In the Er(^{t}Bu$_2$amd)$_3$/O_3 process,[V] the observed growth rate was 0.37–0.55 Å/cycle under the optimized deposition conditions (225–300 °C), but the process was not entirely self-limiting. The Er(^{t}Bu$_2$amd)$_3$/O_3 process and the film properties are discussed more thoroughly in Sections 4.2 and 5.2.

Table 1. ALD processes reported for binary RE oxides. Growth rate values were obtained in the temperature range of the ALD-type growth (column 4).

	Metal precursor	Oxygen source	Dep. Temp. / °C	Growth rate / Å/cycle	Ref.
Sc_2O_3	$Sc(thd)_3$	O_3	335-375	0.13	[89]
	Cp_3Sc	H_2O	250-350	0.75	[89]
	$Sc(^iPr_2amd)_3$	H_2O	225-300	0.7	[109]
Y_2O_3	$Y(thd)_3$	O_3	250-350	0.23	[90-92]
	$Y(thd)_3$	O_2 plasma	300	0.3	[96-98]
	$Y(thd)_3(phen)$	O_3	250-350	0.22	[90]
	$Y(thd)_3(bipy)$	O_3	250-350	0.23	[90]
	Cp_3Y	H_2O	200-350	1.4-1.7	[100]
	$(CpMe)_3Y$	H_2O	200-400	1.2-1.3	[100]
	$Y(^iPr_2amd)_3$	H_2O	150-280	0.8	[109]
La_2O_3	$La(thd)_3$	O_3	225-275	0.36	[93]
	$La[N(SiMe_3)_2]_3$	H_2O	225-275	0.5-0.3 or 4.3	[102-105, 108]
	$La(^iPr_2amd)_3$	H_2O	300*	0.9	[112, 113]
CeO_2	$Ce(thd)_4$	O_3	175-250	0.32	[VI, 94]
	$Ce(thd)_3(phen)$	O_3	225-275	0.42	[VI]
PrO_x	$Pr(mmp)_3$	H_2O	200-300*	0.1-0.7	[99]
	$Pr[N(SiMe_3)_2]_3$	H_2O	200-300*	3.0-0.3	[106]
Nd_2O_3	$Nd(thd)_3$	O_3	270-325	0.45	[I, II]
Sm_2O_3	$Sm(thd)_3$	O_3	300*	0.36	[I]
Eu_2O_3	$Eu(thd)_3$	O_3	300*	0.32	[I]
Gd_2O_3	$Gd(thd)_3$	O_3	250-300	0.30	[I, 95]
	$Gd(mmp)_3$	H_2O	200-250*	0.2-1.0	[99]
	$(CpMe)_3Gd$	H_2O	250-300*	2.1-2.9	[95]
	$Gd[N(SiMe_3)_2]_3$	H_2O	200-250*	0.5-2.2	[107]
Dy_2O_3	$Dy(thd)_3$	O_3	300*	0.31	[I]
Ho_2O_3	$Ho(thd)_3$	O_3	300*	0.25	[I]
Er_2O_3	$Er(thd)_3$	O_3	250-375	0.25	[I, III]
	$Er(thd)_3$	O_2 plasma	300	0.3 or 0.5	[96, 97]
	$(CpMe)_3Er$	H_2O	250-350	1.5	[IV]
	$Er(^tBu_2amd)_3$	O_3	250-300*	0.39-0.55	[V]
Tm_2O_3	$Tm(thd)_3$	O_3	300*	0.22	[I]
Lu_2O_3	$\{[Cp(SiMe_3)]_2LuCl\}_2$	H_2O	360*	0.26	[101]

* = ALD-type growth not observed or not fully studied

3.2.2. ALD of multi-component RE-containing oxides

Besides binary oxides, ALD has been applied for the deposition of thin films containing two or more metals. Basically, the ALD of multi-component oxides is performed by alternately applying the corresponding binary ALD processes. The composition of the films can be controlled by varying the pulsing ratio of the different precursors. The binary processes in question must possess overlapping temperature ranges for ALD-type growth; otherwise the growth of multi-component oxide film will probably not be self-limiting. In theory, the growth rate of multi-component thin films can be calculated from the growth rates of the respective binary ALD processes, but in practise large deviations from the theoretical value are observed. One example is the ALD of $LaAlO_3$.[129] Not only was the growth rate clearly lower than the rate expected on the basis of the binary processes, but the ratio of the observed to the expected growth rate decreased as the number of $La(thd)_3$ cycles increased. This behavior was explained by assuming that the growth of the La-O layer is inhibited by the Al-O layer on the surface or that the bonding mode of $La(thd)_3$ on the Al-O surface differs from that on the La-O surface.

Several multi-component oxide thin films containing at least one RE metal have been deposited by ALD (cf. Table 2). In most cases, studies have aimed at the deposition of ternary oxides, such as perovskites, with defined crystal structure and stoichiometry. There are also examples of RE-containing mixed oxides, which usually are solid solutions of binary oxides with a wide range of metal ratios. In addition, ALD of a structure consisting of distinct layers of La_2O_3 and Al_2O_3, *i.e.* nanolaminate, has been reported.[113]

RE-containing perovskite thin films. In the earliest ALD studies on ternary RE-containing films ($LaNiO_3$ and $LaCoO_3$),[130,131] the approach was to deposit monolayers of the constituent binary oxides, which were expected to intermix and form the desired ternary oxides. Therefore, one deposition cycle consisted of 15 $La(thd)_3/O_3$ pulses followed by 15 pulses of $M(thd)_2/O_3$ (M = Co, Ni). However, the as-deposited La-Ni-O films consisted of separate La-O and Ni-O layers and $LaNiO_3$ was formed only after annealing at 600 °C for 12 hours.[130] As-deposited $LaCoO_3$

films did not consist discrete layers, but they contained slight excess of cobalt, and Co_3O_4 phase was detected after annealing.[131]

Subsequent studies on $LaMnO_3$,[132] $LaAlO_3$,[129] and $LaGaO_3$[133] showed that a better approach is to mix the constituent binary oxides by growing them as sub-monolayers rather than full monolayers. The stoichiometry of the films, *i.e.* ratio of the metals, can be adjusted by changing the pulsing ratio of the constituent oxides. Stoichiometric as-deposited $LaGaO_3$,[133] $LaAlO_3$,[129] and $LaMnO_3$[132] films were obtained, when $La(thd)_3$ and $Ga(acac)_3$, $Al(acac)_3$, or $Mn(thd)_3$ complexes, respectively, were employed as metal precursors. Furthermore, ALD has been applied for the deposition of quaternary films of calcium-substituted lanthanum manganite using $La(thd)_3$, $Ca(thd)_2$, $Mn(thd)_3$, and ozone as precursors.[134] All the as-deposited films were amorphous, but crystalline perovskite phases of $LaGaO_3$, $LaAlO_3$, $LaMnO_3$, and $La_{1-x}Ca_xMnO_3$ were obtained after annealing, a behavior that was typical of most of the ALD-grown multi-component thin films. Amorphous structures of the as-grown multi-component films may be due to low deposition temperatures or impurities in the films.[135]

Neodymium aluminate films have been grown using $Nd(thd)_3$ and $Al(CH_3)_3$ as metal precursors and O_3 and H_2O as oxygen sources.[II] Amorphous and stoichiometric $NdAlO_3$ films were obtained at the deposition temperature of 300 °C, but films crystallized when the annealing temperature was raised to 800–950 °C.

Mixed oxides. The majority of the ALD processes for mixed oxides presented below actually produce solid solutions. Typically, the purpose has been to introduce a controlled amount of doping material into the matrix in order to influence specific properties, such as crystallinity, phase stability, or conductivity. Most of the ALD processes for mixed oxides utilize the $RE(thd)_x/O_3$ processes for binary oxides, but recently other types of RE precursors have been applied as well.

$YScO_3$ is often referred to as yttrium scandate, but in fact it is a solid solution of Y_2O_3 and Sc_2O_3. $YScO_3$ (or Y_2O_3-Sc_2O_3) thin films have recently been grown by ALD using β-diketonates $Y(thd)_3$ and $Sc(thd)_3$ or organometallic $(CpMe)_3Y$ and Cp_3Sc as RE precursors.[136] The growth rate achieved with the Cp precursors and

water (1.07 Å/cycle) was noticeably higher than the rate (0.18 Å/cycle) obtained with thd precursors and ozone. The as-deposited Y_2O_3-Sc_2O_3 films were amorphous but they crystallized as a solid solution after annealing at 800 °C or 1000 °C, depending on the precursors applied. In addition, the films contained only a small amount of impurities and they showed promising electrical properties, the effective permittivity being approximately 15, and higher than that of the constituent oxides.[136]

Thin films of yttria-stabilized zirconia (YSZ, Y_2O_3-ZrO_2), a solid solution formed by Y_2O_3 and ZrO_2, have been deposited by applying $Y(thd)_3$ as yttrium precursor, while $Zr(thd)_4$, Cp_2ZrMe_2, or Cp_2ZrCl_2 has been used as zirconium source.[137] Depending on the precursor combination, surface-controlled ALD-type growth was observed at 275–375 °C, and growth rates of 0.56–0.89 Å/cycle were obtained with Y:Zr precursor pulsing ratio of 1:1. The impurity levels of the YSZ films deposited under optimized conditions were low, the carbon and hydrogen concentrations being typically less than 1 at.-%. With change in the precursor pulsing ratio, the yttria content in Y_2O_3-ZrO_2 varied between 5 and 89 mol-%.[137]

In another study, ALD-grown YSZ films were examined as conducting electrolytes for oxide ions in solid oxide fuel cells (SOFC).[138] Very thick (~3 μm) and dense YSZ films with 8–9 mol-% of Y_2O_3 were deposited from $Y(thd)_3$ and $ZrCl_4$. The suitability of ALD-grown gadolinia-doped cerium oxide or $Ce_{1-x}Gd_xO_{2-0.5x}$ (CGO) films for electrolyte layer in SOFCs has been studied as well.[VII,13] Up to ~1 μm thick CGO films were deposited from $Gd(thd)_3$, $Ce(thd)_4$, and O_3 precursors at 250 °C. The obtained stoichiometry of the films was $Ce_{0.4}Gd_{0.6}O_{1.7}$. The CGO process and analyses of the film properties are described in detail in Sections 4.3 and 5.3.

Radical-enhanced ALD has been utilized for the fabrication of Er_2O_3-doped Y_2O_3 films.[97] Er_2O_3-Y_2O_3 films were deposited at 350 °C from $Er(thd)_3$ and $Y(thd)_3$ metal precursors and oxygen radicals produced in O_2 plasma. The Er content was varied by altering the pulsing ratio of the precursors, but films were reported to contain a significant amount of carbon as an impurity (13 at.-%).

ALD studies on lanthanum aluminum oxide prepared from $La[N(SiMe_3)_2]_3$, trimethylaluminum (TMA), and water were recently reported.[105,108,139] At first, Triyoso *et al.*[105] claimed that owing to the presence of silicon in the lanthanum silylamide precursor, the "La-Al-O" films deposited at 225–275 °C had very high silicon impurity levels and, in fact, the films should be considered as La-Si-Al-O rather than La-Al-O. Later, however, they reported that $LaAlO_3$ films grown by the same process contained less than 1 at.-% of Si.[139] The difference in the results was not mentioned. Kukli *et al.*[108] reported that La-Al-O films grown by the same process contained *ca.* 4 at.-% of silicon. Initially, the silicon impurity was attributed to the Si in the metal precursor,[105] but later, intermixing of the La-Al-O layer and the Si substrate was observed.[139] In another study, $La[N(SiMe_3)_2]_3$ was employed with tris(tertbutoxy)silanol, $(^tBuO)_3SiOH$, to deposit amorphous lanthanum silicate $LaSi_xO_y$, or La_2O_3-SiO_x, but neither the process parameters nor the film properties were discussed in detail.[102]

Nanolaminates. A nanolaminate structure containing La_2O_3 and Al_2O_3 layers has been grown from $La(^iPr_2amd)_3$, TMA, and water.[113] Lanthanum aluminum oxide nanolaminates were reported to contain less than 1 at.-% of carbon and the relative permittivity value was rather good (k = 13). Details of the ALD process and evidence for ALD-type growth were not reported.

Table 2. Reported ALD processes for multi-component RE-containing oxides.

	Metal precursors	Oxygen source	Studied dep. temp. / °C	Ref.
Ternary or quaternary oxides				
$LaNiO_3$	$La(thd)_3 + Ni(thd)_2$	O_3	150-450	[130]
$LaCoO_3$	$La(thd)_3 + Co(thd)_2$	O_3	200-400	[131]
$LaAlO_3$	$La(thd)_3 + Al(acac)_3$	O_3	325-400	[129]
$LaGaO_3$	$La(thd)_3 + Ga(acac)_3$	O_3	325-425	[133]
$LaMnO_3$	$La(thd)_3 + Mn(thd)_3$	O_3	200-400	[132]
$La_{1-x}Ca_xMnO_3$	$La(thd)_3 + Ca(thd)_2 + Mn(thd)_3$	O_3	180-360	[134]
$NdAlO_3$	$Nd(thd)_3 + Al(CH_3)_3$	$O_3 + H_2O$	300	[II]
Mixed oxides				
Y_2O_3 - Sc_2O_3	$Y(thd)_3 + Sc(thd)_3$	O_3	335-350	[136]
	$(CpMe)_3Y + Cp_3Sc$	H_2O	300	[136]
Y_2O_3 - ZrO_2	$Y(thd)_3 + ZrCl_4$	H_2O	400	[138]
	$Y(thd)_3 + Zr(thd)_4$	O_3	375	[137]
	$Y(thd)_3 + Cp_2ZrMe_2$	$O_3 + H_2O$	310-365	[137]
	$Y(thd)_3 + Cp_2ZrCl_2$	$O_3 + H_2O$	275-350	[137]
Er_2O_3 - Y_2O_3	$Er(thd)_3 + Y(thd)_3$	O_2 plasma	300-350	[97]
Gd_2O_3 - CeO_2	$Gd(thd)_3 + Ce(thd)_4$	O_3	250	[VII, 13]
La-Al-Si-O or La-Al-O	$La[N(SiMe_3)_2]_3 + Al(CH_3)_3$	H_2O	225-300	[105,108, 139]
La_2O_3-SiO_x	$La[N(SiMe_3)_2]_3 + (^tBuO)_3SiOH$	H_2O	Not reported	[102]
Nanolaminates				
La_2O_3 / Al_2O_3	$La(^iPr_2amd)_3 + Al(CH_3)_3$	H_2O	300-330	[113]

4. EXPERIMENTAL

This experimental section presents the materials, instruments, and methods employed in the deposition and characterization of the thin films. More detailed descriptions can be found in the original publications I-VII.

4.1. Precursors and substrates

Metal precursors. Three types of metal precursor were utilized in the deposition of lanthanide oxide thin films. Most of the work was done with β-diketonate-type chelates (Fig. 7a, p. 22), namely, thd complexes.[I-III,VI,VII,13,14] In fact, $Ln(thd)_x$ complexes were applied for ALD of all lanthanide oxides except Tb (and Pm) oxide. $Ln(thd)_x$ precursors were also used in the ALD of gadolinium oxide-doped cerium dioxide films. In addition, CeO_2 films were deposited from $Ce(thd)_3(phen)$, which is an adduct of $Ce(thd)_3$. All thd-based precursors were synthesized in the laboratory by literature methods,[119,120] and purified by vacuum sublimation.

Another precursor group studied in this work was cyclopentadienyl (Cp) complexes (Fig. 7c, p. 22). $(CpMe)_3Ce$ and $(CpMe)_3Er$ complexes containing monomethylated Cp ligands and an unsubstituted Cp_3Pr complex were studied for ALD of the respective oxides.[IV,14] $(CpMe)_3Ce$, $(CpMe)_3Er$, and Cp_3Pr were obtained from the Institute of Organometallic Chemistry, Russian Academy of Sciences, Nizhny-Novgorod, Russia. $(CpMe)_3Ce$ was observed to be a highly air and moisture sensitive compound, requiring special attention during loading to the ALD reactor.

Er_2O_3 films were also deposited from an amidinate-type precursor, tris(*N*,*N´*-di-tertbutylacetamidinato)erbium, *i.e.* $Er(^tBu_2amd)_3$, where ligands are coordinated to erbium through nitrogen (Fig. 7f, p. 22).[V] $Er(^tBu_2amd)_3$ was synthesized and characterized by Prof. Charles Winter and his group at Wayne State University, Detroit, Michigan, USA.

Oxygen precursors. Water or ozone was used as the oxygen source. Water could be applied as the oxygen source only when the reactive Cp complexes were used as metal precursors. Water vapor was introduced to the reactor from an external container kept at *ca.* 25 °C. Ozone was required when a less reactive thd based

precursor or the Er-amidinato complex was used as precursor. Ozone was produced from >99.999% oxygen using a Fischer Model 502 ozone generator. The O_3 concentration as determined by iodometric titration was approximately 4 %.[140]

Carrier and purge gases. Nitrogen was used as both carrier and purge gas in all experiments. N_2 was separated from air with a Nitrox UHPN 3000-1 nitrogen generator employing molecular sieve technology and its purity was >99.999%.

Substrates. Most of the films were deposited on 5 cm × 5 cm Si(100) substrates of p- or n-type, which were cut from larger wafers (∅ 150 mm) purchased from Okmetic, Vantaa, Finland. The native oxide on the silicon was not removed before deposition. Ultrasonically cleaned soda lime glass substrates of the same size were usually used as well. However, the main focus of the studies was on the films deposited on Si(100), and all the results presented in this thesis were obtained with those films. CGO films were also deposited onto 2 cm × 2 cm pieces of typical SOFC electrode materials Ni-YSZ and $La_{1-x}Sr_xMnO_3$ (LSM) obtained from InDEC B.V. (Innovative Dutch Electroceramics), Petten, Netherlands.

4.2. Deposition of lanthanide oxide thin films

New ALD processes were developed for several binary lanthanide oxides (CeO_2, Nd_2O_3, Sm_2O_3, Eu_2O_3, Gd_2O_3, Dy_2O_3, Ho_2O_3, Er_2O_3, Tm_2O_3, Yb_2O_3, and Lu_2O_3) and for the mixed oxide of Gd_2O_3 and CeO_2, or $Ce_{1-x}Gd_xO_{2-0.5x}$ (CGO). In addition, ALD of PrO_x was studied. Table 3 summarizes all the processes that were studied, while the typical pulsing sequences used in this work are illustrated in Fig. 8. Depositions were carried out in a satellite version of F-120 research-type ALD reactor (ASM Microchemistry Ltd, Espoo, Finland). The pressure inside the reactor during depositions was *ca.* 2–3 mbar.

Table 3. Sublimation and deposition temperatures, precursor combinations, and substrate materials used in the ALD processes studied in this work. Deposition temperature refers to the range of deposition temperatures studied.

	Precursors	Subl. temp./ °C	Dep. temp./ °C	Ref.
Binary oxides				
CeO_2	$Ce(thd)_4$ / O_3	140	175-375	[VI]
	$Ce(thd)_3(phen)$ / O_3	175-180	225-350	[VI]
	$(CpMe)_3Ce$ / H_2O	120-150	150-300	[14]
PrO_x	$Pr(thd)_3$ / O_3	170-180	200-350	[14]
	Cp_3Pr / H_2O	200-220	230-300	[14]
Nd_2O_3	$Nd(thd)_3$ / O_3	161-164	310	[I, II]
Sm_2O_3	$Sm(thd)_3$ / O_3	148-152	300	[I]
Eu_2O_3	$Eu(thd)_3$ / O_3	135	300	[I]
Gd_2O_3	$Gd(thd)_3$ / O_3	155-160	300	[I]
Dy_2O_3	$Dy(thd)_3$ / O_3	125	300	[I]
Ho_2O_3	$Ho(thd)_3$ / O_3	130	300	[I]
Er_2O_3	$Er(thd)_3$ / O_3	130	200-450	[I, III]
	$(CpMe)_3Er$ / H_2O	115	175-450	[IV]
	$Er(^tBu_2amd)_3$ / O_3	185	225-300	[V]
Tm_2O_3	$Tm(thd)_3$ / O_3	125-128	300	[I]
Yb_2O_3	$Yb(thd)_3$ / O_3	130	300	[14]
Lu_2O_3	$Lu(thd)_3$ / O_3	122-124	200-400	[14]
Multicomponent oxides				
CGO	$Ce(thd)_4$ / O_3 + $Gd(thd)_3$ / O_3	175, 160	250-300	[VII, 13]

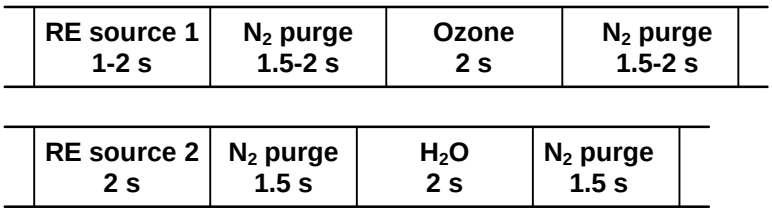

Fig. 8 A diagram of the pulsing sequences used in this work. RE source **1** represents thd and amidinate precursors, while RE source **2** comprises the cyclopentadienyl complexes. Detailed information about the pulsing times in the studied ALD processes can be found in the original publications I-VII.

The preferred stoichiometry and structure of cerium and praseodymium oxides differ from those of other lanthanide oxides studied in this work. This is due to the higher stability of the oxidation state +IV in cerium and praseodymium compounds.[1-3] Cerium preferentially forms fluorite-structured CeO_2, whereas the stoichiometry of praseodymium oxide, PrO_x depends on the prevailing conditions. In fact, praseodymium can form series of intermediate oxides, Pr_nO_{2n-2m}, having fluorite structure. The depositions of CeO_2, PrO_x, and CGO films are presented in separately (Section 4.2.3) since they differed from those of the Ln_2O_3 series.

4.2.1. $Ln(thd)_3/O_3$ process for Ln_2O_3 films

Among the thd-based ALD processes developed for the Ln_2O_3 series, only the growth of Nd_2O_3, Er_2O_3, and Lu_2O_3 films was fully evaluated over a wide temperature range and with different pulsing times of the precursors.[II,III,14] In the depositions of other Ln_2O_3 films (Ln = Sm, Eu, Gd, Dy, Ho, Tm, and Yb), the precursor sublimation temperatures and pulsing times were not optimized but merely set to obtain sufficient precursor flow and surface saturation during the film growth.[I] Furthermore, substrate temperature of 300 °C was used in these depositions because, from the reported ALD processes for RE_2O_3 (RE = Y, La, Nd, or Er),[90,93,II,III] it was clear that the ALD windows of $RE(thd)_3/O_3$ processes are around 300 °C. The thicknesses of the Ln_2O_3 films were adjusted to approximately 50 nm to allow meaningful comparison of the film characteristics, such as purity, roughness, crystallinity, and relative permittivity.[I]

The sublimation temperatures of $Ln(thd)_3$ precursors were observed to decrease toward the heavier lanthanides, from 161−164 °C for $Nd(thd)_3$ to 122 °C for $Lu(thd)_3$. The higher volatility of heavier $Ln(thd)_3$ complexes has been reported earlier.[117,141] Although this finding might at first appear surprising it can be explained in terms of the lanthanide contraction. The smaller size of the heavier lanthanide ions makes their complexes less susceptible to intermolecular interactions such as dimerization and oligomerization, which reduce volatility.[114]

4.2.2. Processes for Er_2O_3 films

Er_2O_3 films were deposited using three different metal precursors.[III-V] In addition to the $Er(thd)_3$ complex, study was made of organometallic $(CpMe)_3Er$ and nitrogen-coordinated $Er(^tBu_2amd)_3$. Er_2O_3 film growth was carefully studied in each process over a wide deposition temperature range and with different pulsing times of the precursors. The suitability of the different precursors for ALD of lanthanide oxides was then evaluated.

Water was used as the oxygen source in the $(CpMe)_3Er$ process, but ozone with $Er(thd)_3$ and $Er(^tBu_2amd)_3$, which do not react with water. Use of water may be preferred for gate dielectric applications since ozone reportedly reacts with HF-etched silicon substrate to form an 1.1–1.4 nm thick interfacial SiO_x layer,[91,142,143] thus increasing the EOT value. This may not be so critical, however, because it might be preferable to have a very thin SiO_2 layer on the Si substrate to obtain dielectric layer of high quality and yet a low EOT value (<1 nm).[144] It has namely been reported that the $HfCl_4/H_2O$ process yielded non-uniform HfO_2 films with poor electrical properties when deposited on H-terminated Si, but high quality films with good electrical properties were obtained when Si substrates had a thin thermally grown SiO_2 layer on top.[145] Additionally, in some comparative studies it has even been reported that H_2O and O_3 form equally thick interfacial SiO_x layers on HF-etched silicon.[142,146]

4.2.3. ALD of CeO_2, $Ce_{1-x}Gd_xO_{2-0.5x}$, and PrO_x films

In the ALD of CeO_2 films, two different β-diketonate compounds, $Ce(thd)_4$ and $Ce(thd)_3(phen)$, were successfully employed as Ce precursors, while ozone was used as the oxygen source. The temperature range studied was 175–375 °C for $Ce(thd)_4$ and 225–350 °C for $Ce(thd)_3(phen)$. The effect of pulse and purge times was investigated as well.[VI] ALD of CeO_2 films was further studied with $(CpMe)_3Ce$ as precursor and a deposition temperature range of 150–300 °C.[14]

The ALD process for $Ce_{1-x}Gd_xO_{2-0.5x}$ (CGO) films[VII,13] was developed by combining the binary $Ce(thd)_4/O_3$[V] and $Gd(thd)_3/O_3$[I,95] processes. The deposition temperature was selected to be 250 °C, which is inside the ALD windows of both binary processes.[VI,95] The aim was to deposit films having the stoichiometry of $Ce_{0.9}Gd_{0.1}O_{1.95}$, and where the conductivity of CGO is highest.[33] CGO films were first deposited on Si(100) substrates to define the dependence of the film stoichiometry on the pulsing ratio of the precursors. Pulsing ratios of $Ce(thd)_4$ and $Gd(thd)_3$ varying from 3:1 to 19:1 were studied. Actual samples for SOFCs were then grown on typical electrode materials: Ni-YSZ cermet and $La_{1-x}Sr_xMnO_3$ (LSM). CGO films were up to 1 μm thick and thus considerably thicker than films in any other study in this work. For comparison, CGO thin films were also prepared by sputtering, and results were compared with those for the ALD-grown films.[VII,13]

Two different precursors were tested for the ALD of PrO_x thin films, namely $Pr(thd)_3$ and Cp_3Pr. The temperature ranges studied were 200–350 °C in the $Pr(thd)_3/O_3$ process and 230–300 °C in the Cp_3Pr/H_2O process.[14]

4.3. Film characterization

Various analytical techniques were employed for characterization of the thin films. Film thicknesses were determined by fitting the transmittance or reflectance spectra measured with a Hitachi U-2000 spectrophotometer.[147] In some cases, thickness of the very thin films was also measured with a Bruker D8 Advance X-ray diffractometer set in the X-ray reflection mode (XRR).

An X-ray diffractometer (Philips MPD 1880) with Cu-Kα radiation was used to determine the crystallinity and crystallite orientation of the films. Fourier transform infrared spectroscopic (FTIR) measurements (Nicolet Magna-IR 750) were carried out to obtain information about hydroxide and carbonate impurities in the films. The contribution of the Si substrate was subtracted from the measured spectra.

Film morphology and uniformity were examined by atomic force microscopy (AFM). A Nanoscope III (Digital Instruments) was used in the AFM measurements and it was operated in tapping mode with a scanning rate of 1–2 Hz. Large area images (10 μm × 10 μm) were measured from different parts of the films to ascertain the uniformity, while final images were taken using a scanning area of 2 μm × 2 μm. Surface roughnesses were calculated as root mean square (rms) values. Furthermore, film composition and stoichiometry were determined by time-of-flight elastic recoil detection analysis (TOF-ERDA).[148,149] A 53 MeV $^{127}I^{10+}$ ion beam produced in a 5 MV tandem accelerator EGP-10-II was used in TOF-ERD analyses.

$Ce_{1-x}Gd_xO_{2-0.5x}$ films were analyzed by combined use of a secondary electron microscope (SEM) and an energy dispersive X-ray spectroscope (EDS) to obtain information about uniformity, density, and stoichiometry. Leica S440 and Tracor-Noran Voyager 1 instruments were used in the SEM and EDS analyses, respectively.

Electrical properties of the dielectric Ln_2O_3 films were analyzed with use of a HP 4284A precision LCR meter for capacitance-voltage (C-V) and a Keitley 2400 Source Meter for current-voltage (I-V) measurements. Al/Ln_2O_3/native SiO_2/n-Si(100)/Al structures for the electrical measurements were prepared by depositing aluminum dots onto the dielectric film surface and an Al-contact layer onto the backside of the Si(100) substrate by electron beam evaporation. The native oxide layer on the backside of the Si(100) substrate was HF-etched before evaporation to achieve ohmic contact between Si and Al. A voltage step of 0.05 V and ac signal frequency of 100 kHz or 500 kHz were used in C-V measurements. A voltage step of 0.05 V was applied in the I-V measurements. Both C-V and I-V measurements were carried out at room temperature and under normal pressure. Electrical conductivity of the CGO films was measured by impedance spectroscopy using an Autolab PGSTAT30 instrument manufactured by Ecochemie BV.

5. RESULTS AND DISCUSSION

The results for ALD of Ln_2O_3, CeO_2, PrO_x, and CGO thin films are now summarized. The growth and properties of Ln_2O_3 films deposited by the $Ln(thd)_3/O_3$ process are discussed in Section 5.1. In Section 5.2, special attention is paid to Er_2O_3 films grown by three different processes. The deposition and properties of CeO_2 and CGO thin films are reviewed in Section 5.3, and finally the ALD of PrO_x films is discussed in Section 5.4.

5.1. Ln_2O_3 thin films from $Ln(thd)_3$ and O_3

The temperature dependence of the growth rate was studied in Nd_2O_3, Er_2O_3, and Lu_2O_3 processes (Fig. 9). A very wide ALD window was achieved in the Er_2O_3 process at 250–375 °C,[III] while the growth rate of Nd_2O_3 and Lu_2O_3 films was nearly constant in narrower ranges of 275–325 °C and 300–350 °C, respectively.[II,14] On the basis of these results, 300 °C was chosen as the deposition temperature for other Ln_2O_3 oxides.

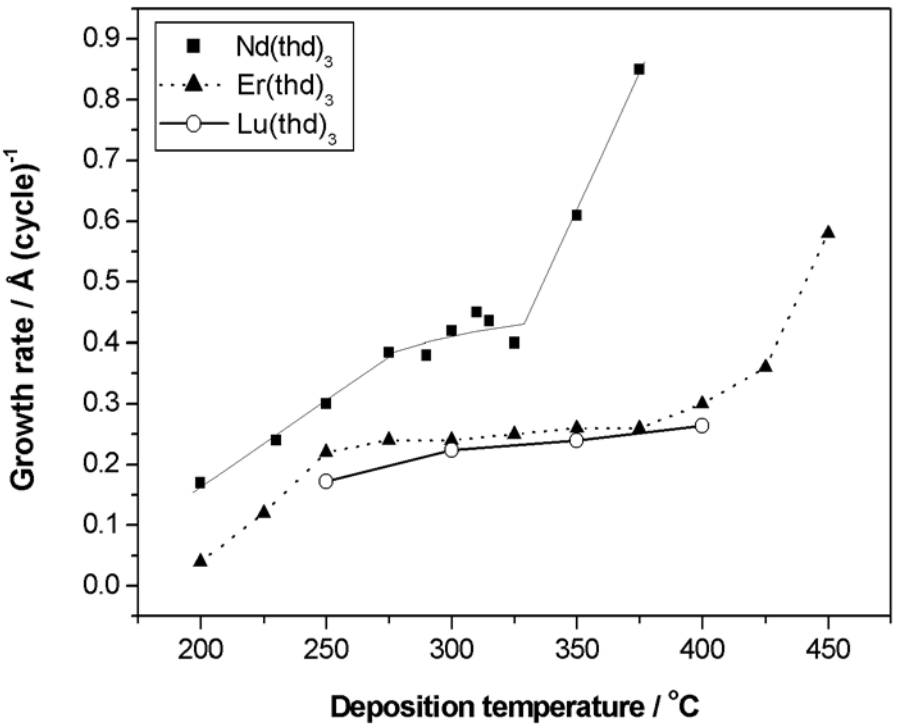

Fig. 9 Growth rates of Nd_2O_3, Er_2O_3, and Lu_2O_3 as a function of deposition temperature.[II,III,14]

The growth rates of the Ln_2O_3 films deposited at 300 °C were in the range of 0.22–0.45 Å/cycle, which corresponds well with the previously reported value of 0.23 Å/cycle for another rare earth oxide, Y_2O_3.[52] The ALD growth rates of the lanthanide oxides decreased with increase in atomic weight of the lanthanide. Since the ionic radius decreases at the same time, a more or less linear dependence is obtained when the growth rates of the Ln_2O_3 thin films are presented as a function of ionic radius (Fig. 10).

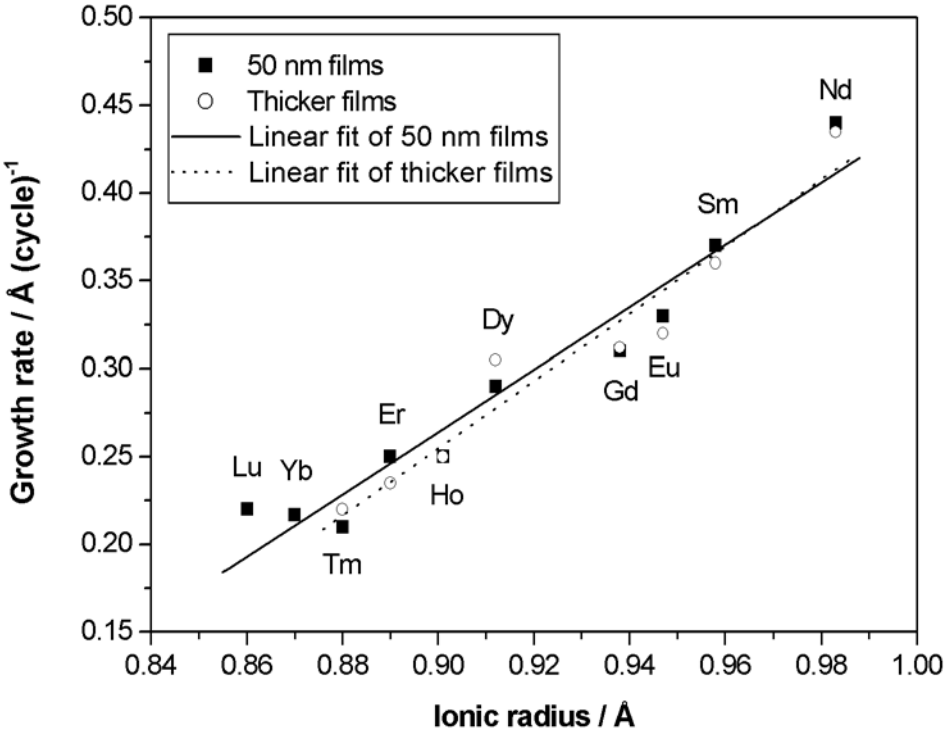

Fig. 10 ALD growth rates of Ln_2O_3 thin films presented as a function of ionic radius.[I-III,14]

The increase in growth rate is large and cannot be fully explained by the increase in ionic radius. For example, the difference between the ionic radii of Tm^{3+} and Gd^{3+} is only 6.8%, while the growth rate of Gd_2O_3 is 45% higher than that of Tm_2O_3. As Puurunen points out,[12] the contribution of the ionic radius is too small alone to explain the increase in growth rate; in addition the number of Ln atoms deposited per cycle per unit surface area has to increase with the ionic radius. The increase in growth rate must thus depend on some factor dependent on the ionic radius. One such factor could be the tendency of larger Ln atoms to adopt high coordination numbers, typically 8 or 9, which results in dimerization of $Ln(thd)_3$ complexes of the

larger lanthanides (Ln = La-Gd).[114,150-152] Complexes of the smaller lanthanides are monomeric.[114,152,153] Such behavior could result in different reactions on the substrate surface. It is not clear what other factors might contribute to the observed trend in growth rate and therefore the ionic radius is the most informative choice at this point.

X-ray diffraction showed the Ln_2O_3 thin films to have a polycrystalline, cubic structure. Films deposited at temperatures close to 300 °C preferred the (100) orientation, as (400) was the strongest observed reflection. Minor (222), (411), (440), (611), and (622) reflections were also detected, as can be seen from the diffraction pattern of Tm_2O_3 presented in Fig. 11a. At 250 °C and below, all studied films were amorphous or only weakly crystalline.[I-III] Studies with Er_2O_3 and Lu_2O_3 showed that, as the deposition temperature was increased, films became more crystalline and the relative intensities of the reflections changed, the (222) reflection being the strongest one above 350 °C (Fig. 11b).[III,14] The same kind of behavior has been reported for Sc_2O_3 and Y_2O_3 films grown by the $RE(thd)_3/O_3$ ALD process when the deposition temperature was increased from 300 °C to 375 °C.[89,90] In the Nd_2O_3 films, however, (100) remained the dominant orientation at all deposition temperatures where crystalline films were obtained (>250 °C).

Lanthanide oxides are basic materials, which become hydrated and carbonated when exposed to atmospheric water and carbon dioxide.[1-3] The basicity increases toward the lighter lanthanides. Neodymium is the lightest of the lanthanides studied in this work, and this may explain why the results for Nd_2O_3 films were somewhat different from those obtained for the other Ln_2O_3 films. For example, the XRD experiments revealed that Nd_2O_3 films react with ambient air during storage and NdO(OH) is formed (Fig. 11c).[II] The formation of NdO(OH) was also observed in FTIR experiments, where an absorption band around 3435 cm^{-1} could be assigned to stretching of the hydroxide group. The tendency of Nd_2O_3 films to absorb water seemed to be related to the amount of carbon impurity in the films. Namely, as the deposition temperature of the Nd_2O_3 films was increased, the carbon concentration decreased (according to FTIR), and at the same time the films became more reactive toward atmospheric moisture. A similar tendency has been reported for ALD-grown La_2O_3 films,[93] but no formation of the LnO(OH) phase was observed for the heavier lanthanide oxides studied here.[I]

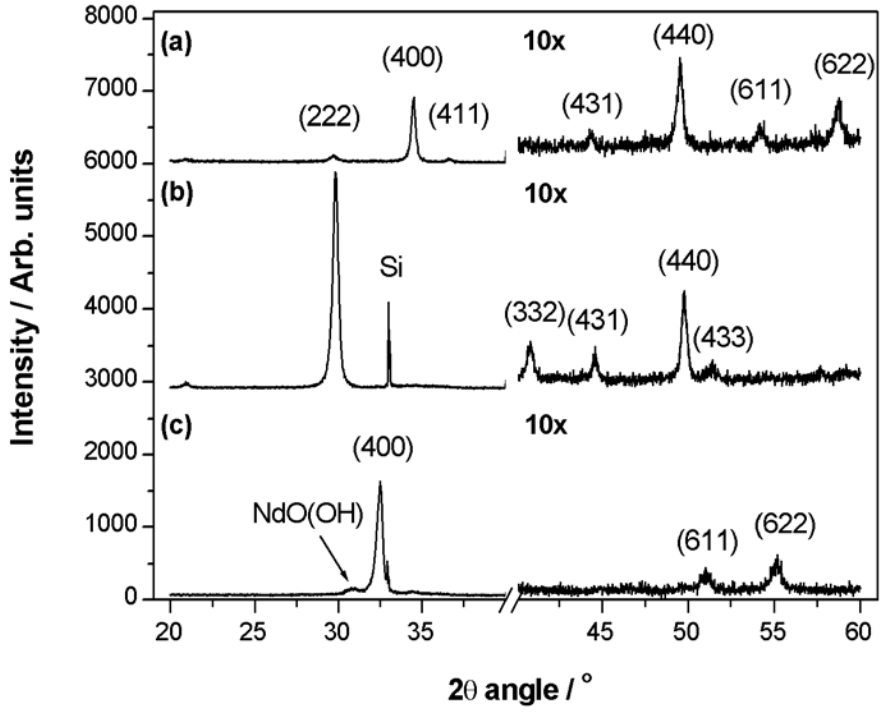

Fig. 11 (a) XRD patterns recorded for a 69-nm Tm_2O_3 film deposited at 300 °C, (b) a 62-nm Lu_2O_3 film deposited at 400 °C, and (c) a 153-nm Nd_2O_3 film deposited at 310 °C after storage of a few months. All the indexed peaks originate from cubic Ln_2O_3 phase, but peaks due to Si(100) substrate or NdO(OH) are also marked in the figure. The signal intensity within the 2θ range of 40–60° is magnified by a factor of ten. XRD patterns were recorded using Cu Kα radiation.

In FTIR measurements of 50-nm thick Ln_2O_3 samples, broad absorption bands appeared at 1400–1600 cm^{-1} due to the asymmetric carbonate C-O stretching.[154-156] This suggested that the carbon impurity was in the form of carbonate species.[I-III,14] Lanthanide oxides, and particularly the lighter Ln_2O_3, are known to react with CO_2.[1-3] In fact, the area of the carbonate absorption peak and therefore the amount of carbonate contamination was observed to decrease toward the heavier lanthanides. Similarly, in studies on Er_2O_3 and Nd_2O_3, the amount of carbon impurity was found to decrease when the deposition temperature was raised.[II,III]

Elemental concentrations in Ln_2O_3 films (Ln = Nd, Sm, Gd, or Er) were measured by TOF-ERDA (Table 4). The main impurity in the films deposited at 300 °C was carbon, which was present at levels ranging from 1.8 to 5.0 at.-%.[I] More detailed studies on Er_2O_3 films showed the carbon concentration to decrease with increasing deposition temperature,[III] in agreement with the FTIR results. When the TOF-ERDA and FTIR results for Nd_2O_3 were considered together, it could be concluded that the films deposited at ≤230 °C actually consisted of neodymium oxycarbonate, $Nd_2O_2CO_3$. A corresponding oxycarbonate phase has previously been detected in La_2O_3 films grown by ALD at low temperatures of 180–275 °C.[93] The formation of the oxycarbonate phase was not observed in Er_2O_3 or Lu_2O_3 films, and the other Ln_2O_3 films were not fully studied. However, since the measured carbonate FTIR peak areas for Nd_2O_3, Sm_2O_3, Eu_2O_3, and Gd_2O_3 films deposited at 300 °C were all of the same magnitude,[I] it may be that these elements form oxycarbonate phase as well, despite the decrease in stability of the lanthanide oxycarbonate phase with increasing atomic number.[157]

Other impurities detected by TOF-ERD analysis of Ln_2O_3 films were hydrogen and fluorine, and Sm_2O_3 films also contained a small amount of sodium. The probable origin of the fluorine impurity was the perfluorinated vacuum grease or Teflon gaskets,[90] while the sodium originated from the sodium hydroxide used in the synthesis of $Sm(thd)_3$.[119] The Ln:O ratios were in the range 0.54–0.63, and thus somewhat below the stoichiometric value of 0.67, but the oxygen excess can partly be explained by the carbonate impurity.

Table 4. Elemental concentrations in Ln_2O_3 (Ln = Nd, Sm, Gd, or Er) films according to TOF-ERDA results.

Material	Temp. / °C	Ln / at.-%	H / at.-%	C / at.-%	O / at.-%	F / at.-%	Na / at.-%	Ln:O ratio
Nd_2O_3	310	34	1.2	4.3	59	1.0	-	0.58
Sm_2O_3	300	32.5	0.6-0.8	5	60	1.1	1.2	0.54
Gd_2O_3	300	33	1.7	2.3	61	1.7-2.0	-	0.54
Er_2O_3	300	36	4	1.8	57	1.7	-	0.63
Er_2O_3	350	36	3	0.8	59	0.8	-	0.61
Er_2O_3	400	36	5	0.5	58	0.7	-	0.62

Lanthanide oxide thin films prepared by the $Ln(thd)_3/O_3$ process appear very smooth and uniform when deposited within the ALD window. For example, according to AFM measurements the rms values of 95-nm-thick Gd_2O_3 and 94-nm-thick Nd_2O_3 films were only 1.9 and 0.8 nm, respectively (cf. Fig. 12).[I,III] Surface roughnesses were not systemically studied, which means that comparisons cannot be made of different Ln_2O_3 films nor of the effects of different deposition conditions. In the case of the $Er(thd)_3/O_3$ process, it was noticed, however, that the surface rougness increases significantly when deposition temperatures above the ALD window are used; the rms value increases from 0.3 nm at 300 °C to 5.6 nm at 400 °C.[III]

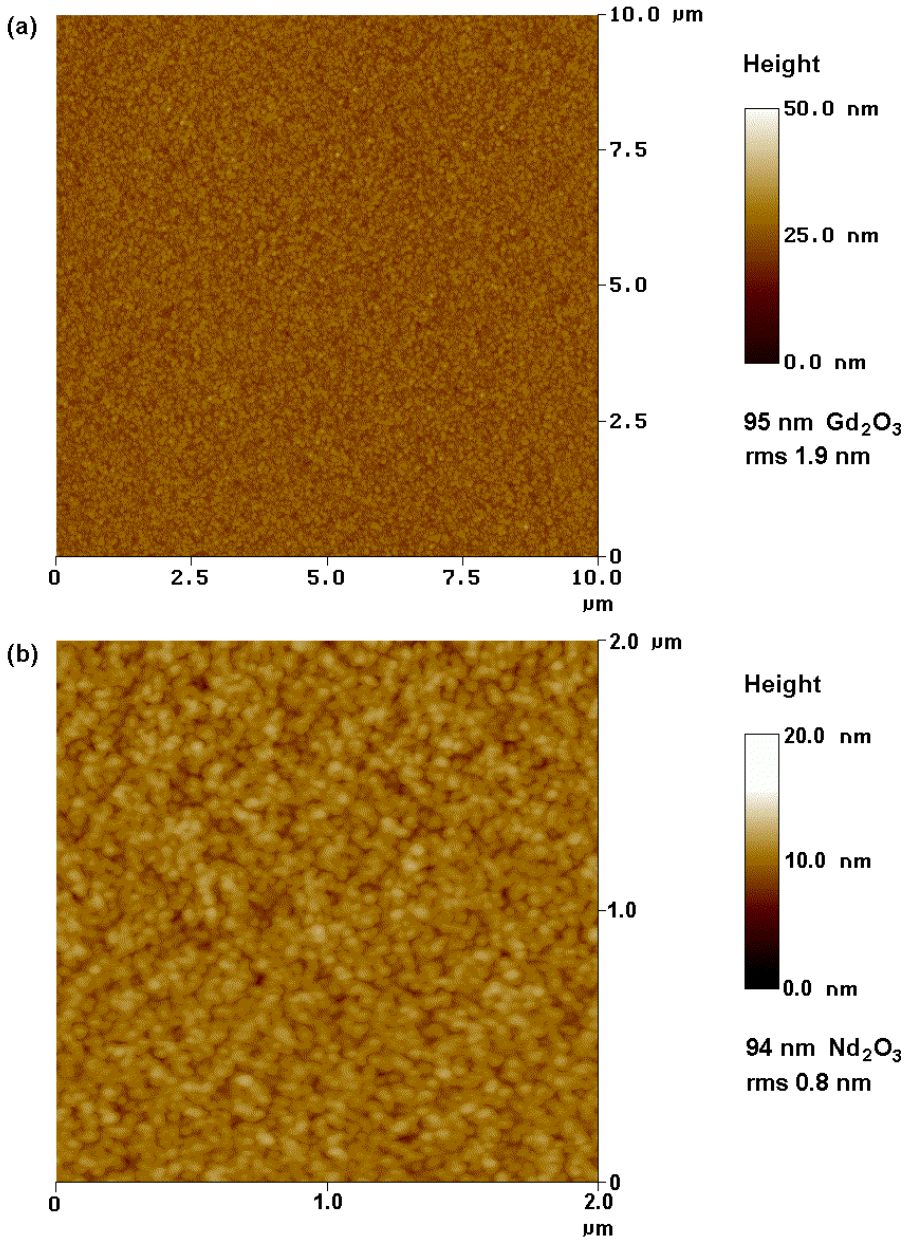

Fig. 12 (a) Two-dimensional AFM images of 95-nm-thick Gd_2O_3 film deposited at 300 °C; image size 10 μm × 10 μm; depth scale 50 nm from black to white; (b) and image of 94-nm-thick Nd_2O_3 film deposited at 310 °C; image size 2 μm × 2 μm; depth scale 20 nm from black to white.

Electrical measurements showed that 50-nm-thick Ln_2O_3 films have rather similar capacitance-voltage (C-V) characteristics (Fig. 13). The relative permittivities of the Al/Si(100)/native SiO_2/Ln_2O_3/Al capacitor structures (Ln = Nd, Sm, Eu, Gd, Dy, Ho, Er, Tm, or Lu) containing the native SiO_2 layer were in the range of 8.4–11.1.[I,14] If the thickness of the interfacial native SiO_2 layer is estimated to be 1.5 nm,[IV] the permittivity values of the Ln_2O_3 layers alone are in the range of 9.0–12.1. These

values correspond fairly well to the literature values of 14.3–12.4 for bulk oxides, although they did not systematically decrease from Nd_2O_3 to Lu_2O_3. The literature values for Ln_2O_3 (Ln = Nd-Lu) thin films prepared by different techniques have typically been in the range of 11-20.[60-66,77,158,159]

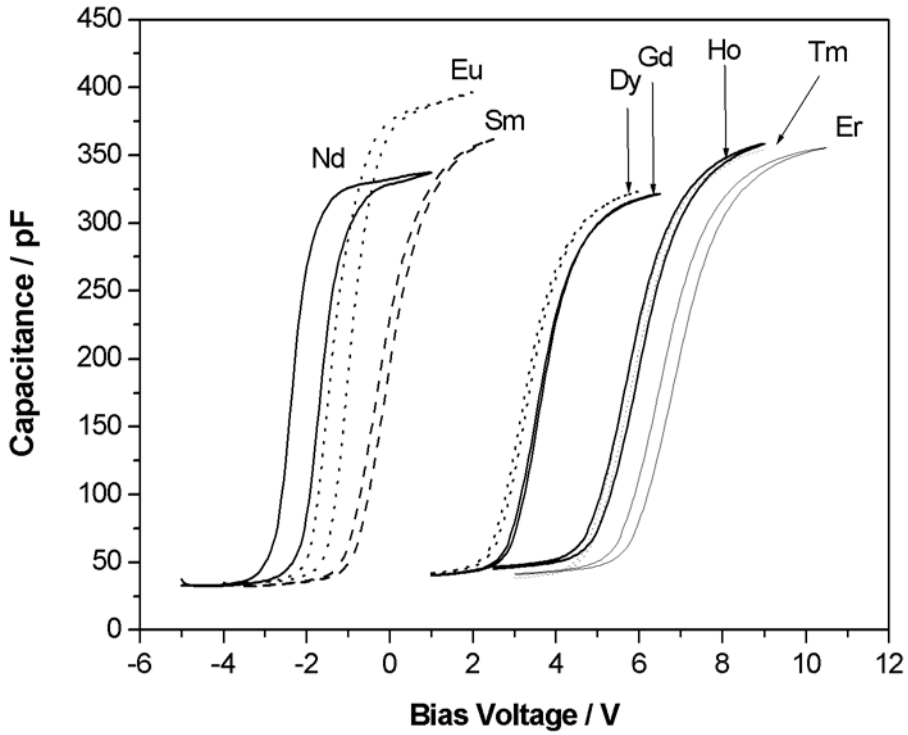

Fig. 13 Capacitance-voltage curves for Al/n-Si(100)/native SiO_2/Ln_2O_3/Al capacitor structures measured with a signal frequency of 500 kHz. Ln_2O_3 (Ln = Nd, Sm, Eu, Gd, Dy, Ho, Er, or Tm) film thickness was approximately 50 nm.[I]

5.2. Er_2O_3 thin films from different processes

The deposition of Er_2O_3 films succeeded from all precursors. Selected characteristics of the different precursors and processes are presented in Table 5 at the end of this section.

From the other ALD studies on thd complexes, it was expected that $Er(thd)_3$ would not react with water, but it was somewhat surprising that no reaction occurred between amidinato complex $Er(^tBu_2amd)_3$ and water, since amidinato complexes $Sc(^iPr_2amd)_3$, $Y(^iPr_2amd)_3$, and $La(^iPr_2amd)_3$ containing smaller isopropyl side groups have been reported to react with water in ALD of the respective oxides.[109-111]

Evidently the larger tertbutyl side groups make the complex more stable, at the same time reducing its reactivity. Details of the processes using RE(^{i}Pr$_2$amd)$_3$ complexes were not given in the literature, however, and it cannot be verified therefore that RE(^{i}Pr$_2$amd)$_3$ complexes are stable enough to produce uniform films through an ALD-like, self-limiting growth mechanism.

Highest growth rate of 1.5 Å/cycle was obtained in the (CpMe)$_3$Er/H$_2$O process. This is about 6 and 3 to 4 times as high as the growth rates in Er(thd)$_3$/O$_3$ and Er(^{t}Bu$_2$amd)$_3$/O$_3$ processes, respectively (see Fig. 14 and Table 5).[III-V] Clear ALD temperature windows were obtained with (CpMe)$_3$Er/H$_2$O and Er(thd)$_3$/O$_3$, but in the Er(^{t}Bu$_2$amd)$_3$/O$_3$ process the growth rate increased with deposition temperature. In the (CpMe)$_3$Er/H$_2$O and Er(thd)$_3$/O$_3$ processes, the growth rate of Er$_2$O$_3$ films remained constant when longer precursor pulse lengths were employed, verifying ALD-type growth. In the Er(^{t}Bu$_2$amd)$_3$/O$_3$ process, however, the growth rate increased slightly with precursor pulse duration suggesting partial thermal decomposition of the precursor.

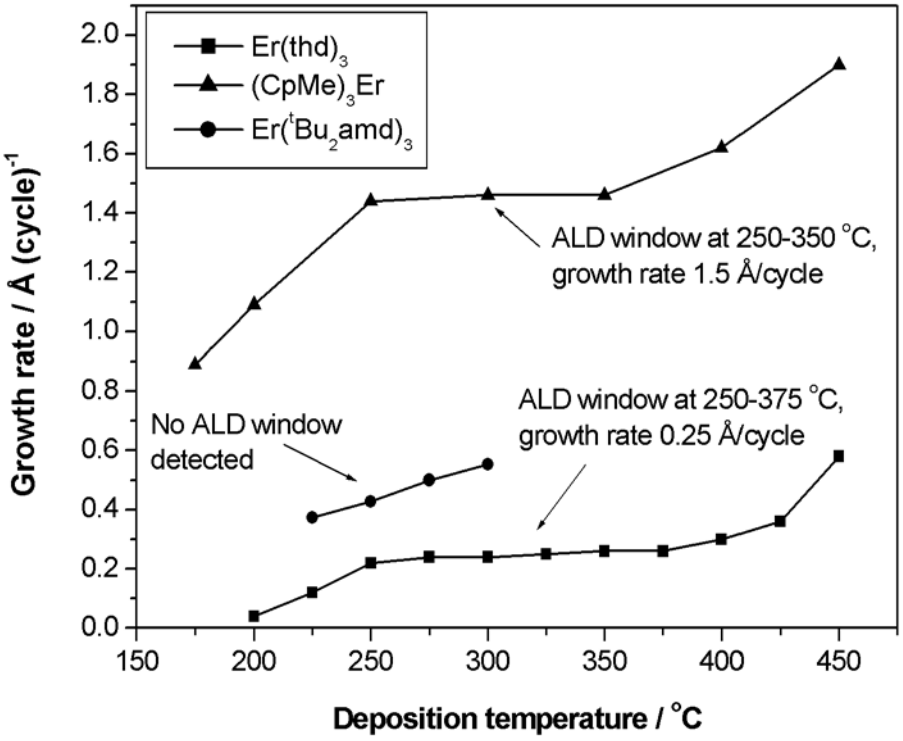

Fig. 14 Growth rates obtained in different ALD processes of Er$_2$O$_3$ as a function of deposition temperature.[III-V]

All processes yielded relatively pure Er_2O_3 films when depositions were performed within the optimized deposition temperature range. According to TOF-ERD analysis, the concentrations of carbon and hydrogen impurities were typically less than 2.0 at.-% and 4.0 at.-%, respectively (Fig. 15 and Table 5). These impurity concentrations are comparable to those reported for RE_2O_3 films grown from corresponding precursors.[89,90,95,100,110] In the case of the $(CpMe)_3Er/H_2O$ process, the carbon level increased with the deposition temperature. In ALD of RE_2O_3, however, the carbon content has typically decreased up to the temperature where precursor decomposition begins.[II,III,89,90,95] As discussed in the previous section, under oxidizing conditions carbon readily forms carbonates in Ln_2O_3 films. FTIR peaks originating from asymmetric carbon-oxygen stretching[154-156] were detected in Er_2O_3 films as well.[III,V] In the $(CpMe)_3Er/H_2O$ process, the formation of the tetragonal $Er_2O_2CO_3$ phase was detected by XRD measurements of Er_2O_3 films deposited at 350-450 °C, where the carbon concentration was high being 2.5–15 at.-%.[IV]

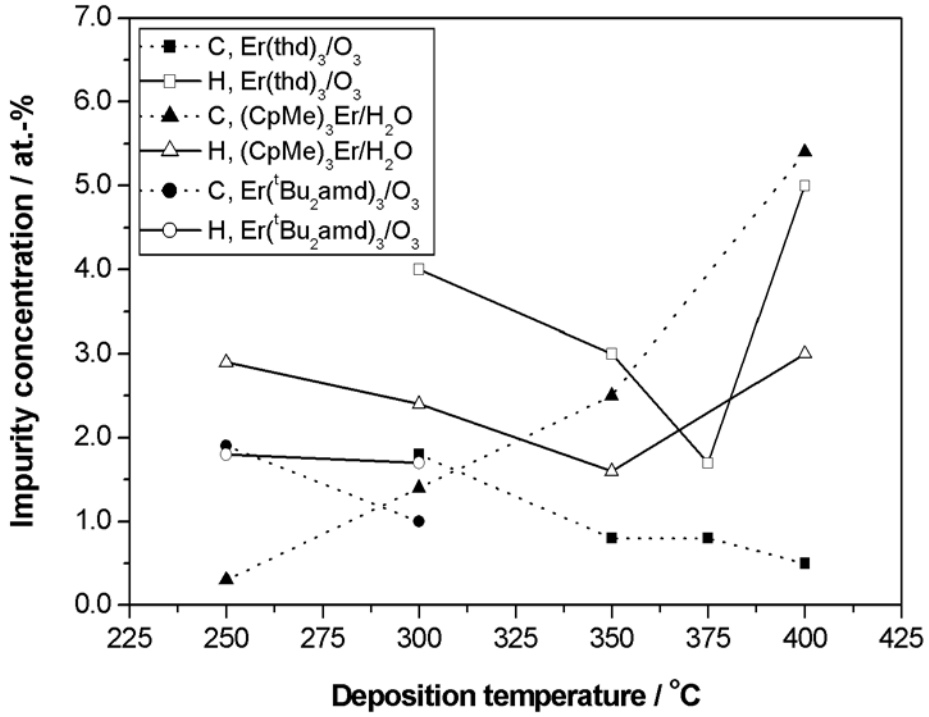

Fig. 15 Concentrations of carbon and hydrogen impurities in Er_2O_3 films deposited by different ALD processes as measured by TOF-ERDA.[III-V]

Crystallinity of the Er_2O_3 films differed slightly according to the process. The as-deposited films grown by $Er(thd)_3/O_3$ and $Er(^tBu_2amd)_3/O_3$ processes were amorphous at deposition temperatures below 250 °C, but they were polycrystalline cubic Er_2O_3 with the (100) orientation dominant when deposited at 250–350 °C. The $(CpMe)_3Er/H_2O$ process, in turn, consistently gave polycrystalline films, the (222) crystal plane showing the strongest reflection throughout the deposition temperature range studied. The (100) and (111) orientations of the cubic Ln_2O_3 phase have been the dominant ones in all previously reported ALD processes as well. Inside the ALD windows of these processes, *i.e.* at deposition temperatures around 300 °C, the $RE(thd)_3/O_3$ process (RE = Y, La, or Nd-Lu)[I-III,90,95] seems to prefer the (100) orientation, but in the case of scandium, which is the smallest RE element, the thd process resulted in (111) oriented Sc_2O_3 films.[89] The (111) orientation is also typically preferred in RE_2O_3 films (RE = Sc, Y, Gd, or Er) grown from cyclopentadienyl precursors.[IV,89,90,95] Where other types of precursors have been used, the dominant orientation in Ln_2O_3 has been (100) in Er_2O_3 from $Er(^tBu_2amd)_3$,[V] (111) in Gd_2O_3 from $Gd(mmp)_3$,[99] and both (111) and (100) in Y_2O_3 from $Y(^iPr_2amd)_3$.[110] The precursor therefore influences the growth mode, and furthermore the orientation of ALD grown films. As noted above, however, in the thd processes the size of the RE ion plays a role as well.

Electrical properties of the 50-nm and 12.5-nm thick Er_2O_3 films grown by the $Er(thd)_3/O_3$ and $(CpMe)_3Er/H_2O$ processes, respectively, were analyzed for permittivity. Films were deposited onto Si(100) substrates covered by a native SiO_2 layer. In both cases, the relative permittivity of the measured Al/Er_2O_3/native SiO_2/p-Si(100)/Al structures was 10. The relative permittivity of the Er_2O_3 layer can only be evaluated if the thickness of the native SiO_2 layer is known. According to XRR measurements, the SiO_2 layer in films grown by the $(CpMe)_3Er/H_2O$ process was *ca.* 1.5 nm thick.[IV] Thus the relative permittivity values were 14.5 and 10.8 for the Er_2O_3 samples deposited by the $(CpMe)_3Er/H_2O$ and $Er(thd)_3/O_3$ processes, respectively. Previously, Mikhelasvili *et al.*[63] have reported relative permittivity values of 6.8 for 6.5-nm-thick and 14 for 50-nm Er_2O_3 films deposited by EBE.

Table 5. Comparison of ALD processes for Er_2O_3 developed in this work.

	$Er(thd)_3/O_3$	$(CpMe)_3Er/H_2O$	$Er(^tBu_2amd)_3/O_3$
Synthesis of the Er precursor	Easy	Complicated (inert atmosphere)	Complicated (inert atmosphere)
Handling of the Er precursor	Easy	Air and moisture sensitive (glove box)	Air and moisture sensitive (glove box)
Availability of the precursor	Commercially available	Commercially available	Not commercially available
Stability under storage	Excellent	Good (glove box)	Good (glove box)
Sublimation temp.	130 °C	115 °C	185 °C
Optimized growth temperature	250-375 °C	250-350 °C	250 °C (ALD window not detected)
Growth rate at 250°C	0.25 Å/cycle	1.5 Å/cycle	0.45 Å/cycle
Impurities in the films deposited in optimized. temp. range	<1.8 at.-% C <4.0 at.-% H <1.7 at.-% F [a]	<2.5 at.-% C <2.9 at.-% H F not detected	<1.8 at.-% C <1.9 at.-% H <1.3 at. % F [a]
Er to O ratio	0.59-0.63	0.58-0.59	0.55-0.59

[a] For origin of F, see the text p.46 or Ref. 90.

5.3. CeO_2 and $Ce_{1-x}Gd_xO_{2-0.5x}$ thin films

Both $Ce(thd)_4$ and $Ce(thd)_3(phen)$ can be used as cerium precursors to deposit CeO_2 films by ALD.[VI] Regions of constant growth rate were obtained at 175–275 °C in the $Ce(thd)_4/O_3$ process and at 225–275 °C in the $Ce(thd)_3(phen)/O_3$ process. Within the ALD windows of both processes, CeO_2 films were polycrystalline and the (111) orientation of the fluorite-structured, cubic CeO_2 was dominant. Films were highly uniform, as the rms values of 50–75-nm-thick films were in the range of 0.6–1.2 nm.

According to TOF-ERD analysis, the CeO_2 films deposited from $Ce(thd)_4$ or $Ce(thd)_3(phen)$ precursors at 200–225 °C contained 0.8–4.0 at.-% carbon, 7–10 at.-% hydrogen, and 1.3–2.0 at.-% fluorine as impurities (Table 6). The high hydrogen concentrations are probably due to the relatively low deposition temperatures of the

sample films, as is typical for thd processes.[III,90,95] The presence of carbon was verified by FTIR measurements, where a carbonate-type impurity was observed.

The growth rate obtained with $Ce(thd)_3(phen)/O_3$ (0.42 Å/cycle) was somewhat higher than that of the $Ce(thd)_4/O_3$ process (0.32 Å/cycle). Otherwise the $Ce(thd)_4$ precursor seemed better. The advantages of $Ce(thd)_4$ include its stability under storage and the width of the ALD window. Furthermore, $Ce(thd)_4$ is more easily and more reproducibly synthesized (see Table 6), although its physical and chemical properties are also known to depend on the method of synthesis.[160]

The third Ce precursor studied in this work was organometallic $(CpMe)_3Ce$. However, $(CpMe)_3Ce$ is too air and moisture sensitive to be used as an ALD precursor, at least if an inert precursor loading system is not available and the precursor is exposed to air even for a short period of time.[14] Films prepared from this precursor had a visually observable thickness profile and were dark colored suggesting a high level of carbon impurity. A comparison of the three CeO_2 processes is presented in Table 6.

Table 6. Comparison of ALD precursors for CeO_2 studied in this work.

	$Ce(thd)_4$	$Ce(thd)_3(phen)$	$(CpMe)_3Ce$
Synthesis of the precursor	Easy, but problems in reproducibility	Easy, but problems in reproducibility	Complicated (inert atmosphere)
Handling of the precursor	Easy	Easy	Highly air and moisture sensitive
Commercially available	Yes	No	Yes
Stability under prolonged storage	Good	Fair	Good (glove box)
Sublimation temp.	140 °C	175-180 °C	125-150 °C
Growth temperature (ALD window)	175-275 °C	225-275 °C	- [a]
Growth rate at 250°C	0.32 Å/cycle	0.42 Å/cycle	- [a]
Impurities in CeO_2 film deposited at 225 °C	0.8 at.-% C 7.0 at.-% H 2.0 at.-% F [b]	4.0 at.-% C 9.0 at.-% H 0.6 at.-% F [b] 0.4 at.-% Na [c]	Not measured
Ce to O ratio	0.47	0.46	Not measured

[a] Depositions did not succeed, see text above; [b] For origin of F, see text p. 46 or Ref. 90;

[c] Na originates from the precursor synthesis, see Ref. 119.

The growth rate of CGO films deposited with the $Ce(thd)_4/O_3/Gd(thd)_3/O_3$ process was approximately 0.40 Å/cycle.[VII] On the basis of preliminary studies on Si(100), the pulsing ratio of $Ce(thd)_4$ and $Gd(thd)_3$ was adjusted in order to obtain the stoichiometry of $Ce_{0.9}Gd_{0.1}O_{1.95}$, where conductivity is at maximum. According to EDS analyses, however, the actual SOFC samples deposited onto LSM and Ni-YSZ substrates contained excess of Gd and the film stoichiometry was $Ce_{0.4}Gd_{0.6}O_{1.7}$. Comparison of the electrical properties of the ALD-grown CGO electrolyte layers with those of sputtered CGO films having the optimal stoichiometry of $Ce_{0.9}Gd_{0.1}O_{1.95}$[13] revealed noticeably higher conductivity for the sputter-deposited films. On the positive side, the ALD-grown CGO films were uniform, very dense, and conformal following closely the shapes of the substrate surface (Fig. 16).

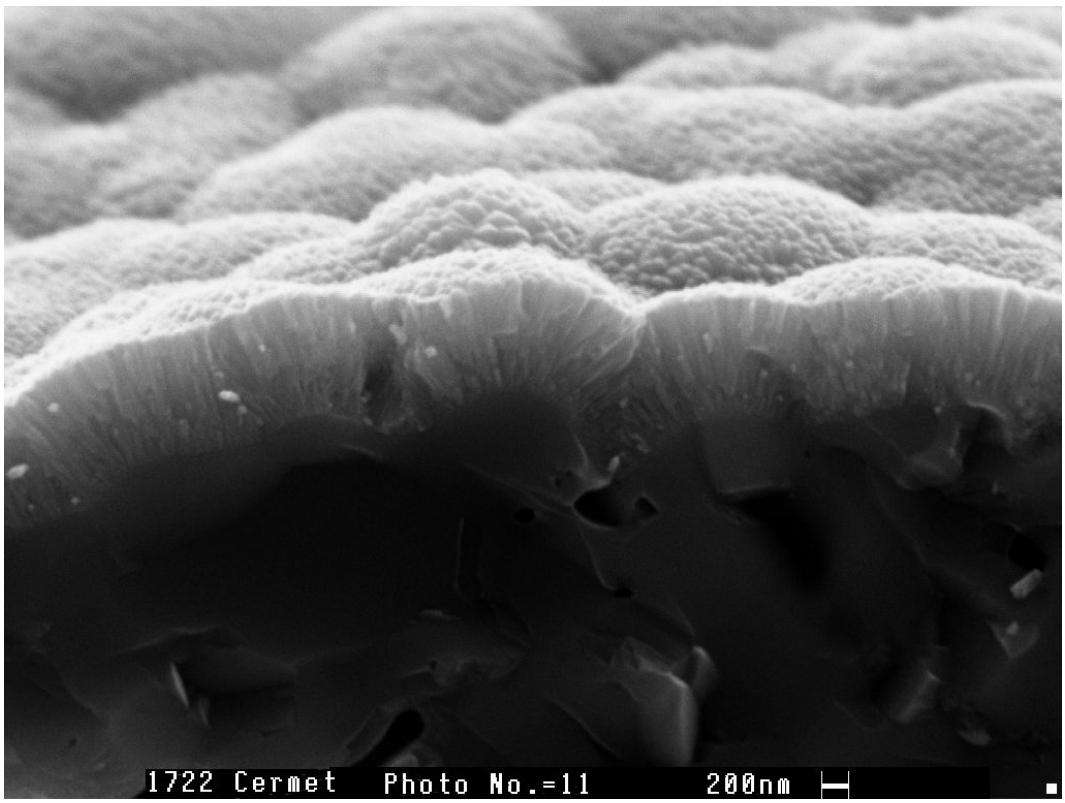

Fig. 16 Cross-sectional SEM view of an ALD-grown 1-µm-thick $Ce_{0.4}Gd_{0.6}O_{1.7}$ thin film on LSM substrate.[VII]

In the future, the stoichiometry of CGO needs to be adjusted to achieve better ionic conductivity.[VII,13] In addition, it might be preferable to develop an ALD process for CGO with a higher growth rate, because electrolyte layers in SOFCs are at least several hundred nanometers thick. Until different precursor combinations leading to higher growth rates are developed, the use of ALD in SOFC technology may be limited to the deposition of thin interlayers between electrodes and the electrolyte.

5.4. PrO_x thin films

Good quality PrO_x films could not be grown from the precursors studied in this work. When $Pr(thd)_3$ and O_3 were used as precursors, the films exhibited a distinct thickness profile at all temperatures studied.[14] The growth rate increased from 0.38 Å/cycle at 190 °C to 1.48 Å/cycle at 350 °C. In terms of thickness uniformity, the best films were obtained at the lower end of the deposition temperature range. At 200 °C, growth rate increased from 0.52 Å/cycle to 0.71 Å/cycle as the $Pr(thd)_3$ pulse length was increased from 0.5 s to 3.75 s. Elemental analyses of PrO_x were not carried out, but reported RE oxide thd processes,[I-III,VI,89,90] suggest that the impurity

concentrations are rather high at low deposition temperatures, and somewhat higher temperatures should be preferred.

Depositions from Cp_3Pr and H_2O resulted in non-uniform films. Films had a clearly visible thickness profile at deposition temperatures of 230–300 °C.[14] Note, however, that the sublimation temperature of Cp_3Pr was high, 200–220 °C. The low volatility of Cp_3Pr was probably due to attractive forces between the neighboring molecules which may have led to oligomerization. Intermolecular forces should be inhibited by adding side groups to Cp ring thus enhancing the volatility.

6. CONCLUSIONS

The ALD studies reported here on the deposition of lanthanide oxide thin films covered most of the lanthanides (Ce-Lu). Studies with different metal precursors gave valuable information about their suitability for ALD precursors. In the following, the main features of the different processes are summarized and conclusions regarding the processes are presented.

$Ln(thd)_3$ complexes were demonstrated to be viable precursors in ALD. Deposition processes were developed for the majority of the lanthanides in the Ln_2O_3 series, and some general features can be noted: (i) Thd complexes are not reactive toward water but require the use of a strong oxidizer, such as ozone, for completion of surface reactions. This may be a problem in high-k applications where the formation of interfacial SiO_2 layer increases the EOT value. (ii) The optimal deposition temperatures, *i.e.* the ALD window, are typically aout 300 °C. Low deposition temperatures should be suitable for a number of applications. (iii) Growth rates are relatively low, ranging from 0.22 Å/cycle for Lu_2O_3 to 0.45 Å/cycle for Nd_2O_3. Although low growth rate is not critical in applications utilizing very thin films over a large substrate area, it may limit the use of thd processes in applications such as SOFCs that require thicker films (~1 μm).

Results obtained with the $(CpMe)_3Er$ precursor were highly encouraging: high quality lanthanide oxide films with good electrical properties were grown by an ALD process having water as an oxygen precursor. $(CpMe)_3Ce$ and Cp_3Pr could not be employed as precursors in ALD of their respective oxides. In future, studies on cyclopentadienyl precursors may play an important role in high-k research, if, as seems probable, water-based processes are developed for lighter lanthanide oxides with larger permittivity values. It seems that, in the case of the heavier (but smaller) lanthanides such as erbium, the Cp ring does not need to be highly substituted, but a single methyl group is sufficient to stabilize the complex. Lighter and larger lanthanides, in turn, need bulkier substituents to make their complexes thermally stable. Substituents in the Cp ring also make complexes more volatile by preventing their dimerization and oligomerization.

On the basis of the present studies, $(CpMe)_3Er$ can be considered as the best Er precursor for ALD of Er_2O_3. Among the three Er precursors tested for the ALD of Er_2O_3, $(CpMe)_3Er$ was associated with highest growth rate, lowest impurity levels, and highest relative permittivity values. However, impurity levels were also very low for Er_2O_3 films deposited by the $Er(thd)_3/O_3$ and $Er(^tBu_2amd)_3/O_3$ processes. Er_2O_3 films deposited by the $Er(thd)_3/O_3$ and $(CpMe)_3Er/H_2O$ processes under optimized conditions were highly uniform, but the films from the $Er(^tBu_2amd)_3/O_3$ process had a slight thickness profile.

Atomic layer deposition of CeO_2 was achieved with two different precursors: β-diketonate-type $Ce(thd)_4$ and $Ce(thd)_3(phen)$. Comparison of these two precursors showed that adducting does not bring any distinct advantages to ALD of CeO_2. Although the growth rate achieved in the $Ce(thd)_3(phen)/O_3$ process was higher than that of the $Ce(thd)_4/O_3$ process, the synthesis of $Ce(thd)_3phen$ was more complicated and less reproducible. The deposition of $Ce_{1-x}Gd_xO_{2-0.5x}$ mixed oxide was initiated on the basis of the previously studied binary processes for CeO_2 and Gd_2O_3, but the stoichiometry of the CGO films could not be properly adjusted during the course of this work. Nevertheless, the CGO films prepared by ALD were of high quality, being very dense and conformal. More work now needs to be done to achieve optimal stoichiometry and to develop an ALD process with higher growth rate, since the electrolyte layers need to be relatively thick.

REFERENCES

1. Greenwood, N.N. and Earnshaw, A., *Chemistry of the Elements*, 2nd Ed., Butterworth-Heinemann, Oxford 1997, pp. 1227-1249.
2. Haire, R.G. and Eyring, L., In: *Handbook on the Physics and Chemistry of Rare Earths, Vol. 18*, (Eds. K.A., Gschneider Jr, L. Eyring, G.R. Choppin, G.R. Lander), Elsevier, Amsterdam 1994, pp. 413-505.
3. Adachi, G.-Y. and Imanaka, N., *Chem. Rev.* **98** (1998) 1479.
4. Hedrick, J.B., In: *U.S. Geological Survey, Mineral Commodity Summaries*, January 2001, pp. 130-131.
5. Xue, D., Betzler, K., and Hesse, H., *J. Phys.: Condens. Matter* **12** (2000) 3113.
6. Schlom, D.G. and Haeni, J.H., *Mater. Res. Soc. Bull.* **27** (2002) 198.
7. Leskelä, M. and Ritala, M., *J. Solid State Chem.* **171** (2003) 170.
8. Leskelä, M., Kukli, K., and Ritala, M., *J. Alloys Compd* (2006) In press.
9. Iwai, H., Ohmi, S., Akama, S., Kikuchi, A., Kashiwagi, I., Ooshima, C., Taguchi, J., Yamamoto, H., Kobayashi, C., Sato, K., Takeda, M., Oshima, K., and Ishiwara, H., In: *Future Trends in Microelectronics* (Eds. S. Luryi, J. Lu, A. Zaslavsky), John Wiley & Sons, New York 2002, pp. 55-62.
10. *International Technology Roadmap for Semiconductors*, http://public.itrs.net/, 9.1.2006.
11. Ritala, M. and Leskelä, M., In: *Handbook of Thin Film Materials* (Ed. H.S. Nalwa), Academic Press, San Diego 2002, pp. 103-159.
12. Puurunen, R., *J. Appl. Phys.* **97** (2005) 121301.
13. Gourba, E., Ringuedé, A., Cassir, M., Billard, A., Päiväsaari, J., Niinistö, J., Putkonen, M., and Niinistö, L., *Ionics* **9** (2003) 15.
14. Päiväsaari, J., Unpublished results.
15. Moore, G.E., *Electronics* **38** (1965) 114.

16. Bersuker, G., Zeitzoff, P., Brown, and Huff, H.R., *Mater. Today* **(2004)** Jan., 26.

17. Wilk, G.D, Wallace, R.M., and Anthony, J.M., *J. Appl. Phys.* **89** (2001) 5243.

18. Thakur, R.P.S., Chen, Y., Poindexter, E.H., and Singh, R., *Electrochem. Soc. Interface* **8** (1999) 20.

19. Singh, R. and Ulrich, R.K., *Electrochem. Soc. Interface* **8** (1999) 26.

20. Hubbard, K.J. and Schlom, D.G., *J. Mater. Chem.* **11** (1996) 2757.

21. Yeo, Y.-C., King, T.-J., and Hu, C., *Appl. Phys. Lett.* **81** (2002) 2091.

22. Houssa, M. (Ed.), *High-κ Gate Dielectrics*, IOP publishing, Bristol 2004, p. 597.

23. Hand, A., *Semicond. Int.* **26** (2003) 46.

24. Pearson, A.D., MacChesney, J.B., and French, W.G., In: *Kirk-Othmer Encyclopedia of Chemical Technology*, *Vol. 10*, John Wiley & Sons, New York 1980, pp. 125-147.

25. Nakahara, T., Hoshikawa, M., Sugawa, T., and Watanabe, M., In: *Ullmann's Encyclopedia of Industrial Chemistry*, *Vol. A10*, (Ed. W. Gerhartz), VCH, Weinheim 1987, pp. 433-449.

26. Polman, A. and van Veggel, F.C.J.M., *J. Opt. Soc. Am. B* **21** (2004) 871.

27. Miniscalco, W.J., *J. Lightwave Technol.* **9** (1991) 234.

28. Van den Hoven, G.N., Koper, R.J.I.M., Polmna, A., van Dam, C., van Uffelen, J.W.M., and Smit, M.K., *Appl. Phys. Lett.* **68** (1996) 1886.

29. Solehmainen, K., Kapulainen, M., Heimala, P., and Polamo, K., *IEEE Photon. Technol. Lett.* **16** (2004) 194.

30. Cassir, M. and Gourba, E., *Ann. Chim. Sci. Mat.* **26** (2001) 49.

31. Inaba, H. and Tagawa, H., *Solid State Ionics* **83** (1996) 1.

32. Gödickemeier, M. and Gauckler, L.J., *J. Electrochem. Soc.* **145** (1998) 414.

33. Steele, B.C.H., *Solid State Ionics* **129** (2000) 95.

34. Steele, B.C.H., *Solid State Ionics* **134** (200) 3.

35. Arachi, Y., Sakai, H., Yamamoto, O, Takeda, Y., and Imahishai, N., *Solid State Ionics* **121** (1999) 133.

36. Cook, R.L., Osborne, J.J., White, J.H., MacDuff, R.C., and Sammells, A.F., *J. Electrochem. Soc.* **139** (1992) L19.

37. Sammes, N.M., Tompsett, G.A., Näfe, H., and Aldinger, F., *J. Eur. Ceram. Soc.* **19** (1999) 1801.

38. Kudo, T. and Obayashi, H., *J. Electrochem. Soc.* **122** (1975) 142.

39. Christie, G.M. and van Berkel, F.P.F., *Solid State Ionics* **83** (1996) 17.

40. Faber, J. Geoffroy, C., Roux, A., Sylvestre, A., and Abelard, P., *Appl. Phys. A* **49** (1989) 225.

41. Van Herle, J., Horita, T., Kawada, T., Sakai, N., Yokokawa, H. and Dokiya, M., *Solid State Ionics* **86-88** (1996) 1255.

42. Huang, W., Shuk, P., and Greenbaltt, M., *Solid State Ionics* **113-115** (1998) 305.

43. Steele, B.C.H. and Heinzel, A., *Nature* **414** (2001) 345.

44. Charpentier, P., Fragnaud, P., Schleich, D.M., and Gehain, E., *Solid State Ionics* **135** (2000) 373.

45. Tsai, T. and Barnett, S.A., *Solid State Ionics* **98** (1997) 191.

46. Bohac, P. and Gauckler, L., *Solid State Ionics* **119** (1999) 317.

47. Song, H.Z., Wang, H.B., Zha, S.W., Peng, D.K., and Meng, G.Y., *Solid State Ionics* **156** (2003) 249.

48. Doshi, R., von Richards, L., Carter, J.D., Wang, X., and Krumpelt, M., *J. Electrochem. Soc.* **146** (1999) 1273.

49. Tsoga, A., Gupta, A., Naoumidis, A., and Nikolopoulos, P., *Acta Mater.* **48** (2000) 4709.

50. Niinistö, L., Päiväsaari, J., Niinistö, J., Putkonen, M., and Nieminen, M., *Phys. Stat. Sol. A* **201** (2004) 1443.

51. Niinistö, L., Ritala, M., and Leskelä, M., *Mater. Sci. Eng. B* **41** (1996) 23.

52. Putkonen, M., *Development of Low-temperature Deposition Processes by Atomic Layer Epitaxy for Binary and Ternary Oxide Thin Films*, Ph.D. Thesis, Helsinki University of Technology, Helsinki 2002, 69 p.

53. Rahtu, A., *Atomic Layer Deposition of High Permittivity Oxides: Film Growth and In Situ Studies*, Ph. D. Thesis, University of Helsinki, Helsinki 2002, 69 p.

54. Niinistö, J., Rahtu, A., Putkonen, M., Ritala, M., Leskelä, M., and Niinistö, L., *Langmuir* **21** (2005) 7321-7325.

55. Liu, X., Ramanathan, S., Longdergan, A., Srivastava, A., Lee, E., Seidel, T.E., Barton, J.T., Pang, D., and Gordon, R.G., *J. Electrochem. Soc.* **152** (2005) G213.

56. Kim, S.K., Hwang, C.S., Park, S.-H.K., and Yun, S.J., *Thin Solid Films* **478** (2005) 103.

57. Puurunen, R.L., *Chem. Vap. Deposition* **9** (2003) 327.

58. Suntola, T., In: *Handbook of Thin Film Process Technology* (Ed. D.A. Glocker), IOP Publishing Ltd, London 1995, pp. B1.5:1-17.

59. Ritala, M., Leskelä, M., Dekker, J.-P., Mutsaers, C., Soininen, P.J., and Skarp, J., *Chem. Vap. Deposition* **5** (1999) 7.

60. Ohmi, S., Takeda, M., Ishiwara, H., and Iwai, H., *J. Electrochem. Soc.* **151** (2004) G279.

61. Ohmi, S., Kobayashi, C., Kashiwagi, I., Ohsima, C., Ishiwara, H., and Iwai, H., *J. Electrochem. Soc.* **150** (2004) F134.

62. Landheer, D., Gupta, J.A., Sproule, G.I., McCaffrey, J.P., Graham, M.J., Yang, K.-C., Lu, Z.-H., and Lennard, W.N., *J. Electrochem. Soc.* **148** (2001) G29.

63. Mikhelasvili, V., Eisenstein, G., Edelman, F., Brener, R., Zakharov, N., and Werner, P., *J. Appl. Phys.* **95** (2004) 613.

64. Jeon, S., Im, K:, Yang, H., Lee, H., Sim, H., Choi, S., Jang, T., and Hwang, H., *Proc. International Electron Devices Meeting 2001, IEDM Technical Digest* (2001) 20.6.1.

65. Wiktorczyk, T., *J. Electrostat.* **51-52** (2001) 131.

66. Li, Y.-L., Chen, N.-F., Zhou, J.-P., Song, S.-L., Liu, L.-F., Yin, Z.-G., and Cai, C.-L., *J. Cryst. Growth* **265** (2004) 548.

67. Ono, H. and Katsumata, T., *Appl. Phys. Lett.* **78** (2001) 1832.

68. Shiokawa, Y., Amano, R., Nomura, A., and Yagi, M., *J. Radioanal. Nucl. Chem.* **152** (1991) 373.

69. Becht, M., Gerfin, T., and Dahmen, K.-H., *Chem. Mater.* **5** (1993) 137.

70. Sharma, R.N. and Rastogi, A.C., *J. Appl. Phys.* **74** (1993) 6691.

71. Bonnet, G., Lachkar, M., Larpin, J.P., and Corson, J.C., *Solid-State Ionics* **72** (1994) 344.

72. Tasaki, Y., Satoh, M., Yoshizawa, S., Kataoka, H., and Hidaka, H., *Jpn. J. Appl. Phys.* **36** (1997) 6871.

73. Lo Nigro, R., Toro, R.G., Malandrino, G., Raineri, V., and Fragalà, I.L., *Adv. Mater.* **15** (2003) 1071.

74. Cheng, J.-B., Li, A.-D., Shao, Q.Y., Ling, H.-Q., Wu, D., Wang, Y., Bao, Y.-J., Wang, M., Liu, Z.-G., and Ming, N.-B., *Appl. Surf. Sci.* **233** (2004) 91.

75. Lo Nigro, R., Toro, R.G., Malandrino, G., Raineri, V., and Fragalà, I.L., *Mater. Sci. Eng. B* **118** (2005) 117.

76. Weber, A. and Suhr, H., *Mod. Phys. Lett.* **3** (1989) 1001.

77. Song, M.-K. and Rhee, S.-W., *Thin Solid Films* **492** (2005) 19.

78. Fleeting, K.A., Davies, H.O., Jones, A.C., O'Brien, P., Leedham, T.J., Crosbie, M.J., Wright, P.J., and Williams, D.J., *Chem. Vap. Deposition* **5** (1999) 261.

79. Kang, S.-W. and Rhee, S.-W., *J. Electrochem. Soc.* **149** (2002) C345.

80. McAleese, J., Plakatouras, J.C, and Steele, B.C.H., *Thin Solid Films* **286** (1996) 64.

81. Singh, M.P., Shalini, K., and Shivashankar, S.A., *Proc. Electrochem. Soc.* **2003-08** (2003) 821.

82. Singh, M.P. and Shivashankar, S.A., *J. Cryst. Growth* **276** (2005) 148.

83. Aspinall, H.C., Gaskell, J., Williams, P.A., Jones, A.C., Chalker, P.R., Marshall, P.A., Smith, L.M., and Critchlow, G.W., *Chem. Vap. Deposition* **10** (2004) 13.

84. Aspinall, H.C., Gaskell, J., Williams, P.A., Jones, A.C., Chalker, P.R., Marshall, P.A., Bickley, J.F., Smith, L.M., and Critchlow, G.W., *Chem. Vap. Deposition* **9** (2003) 235.

85. Aspinall, H.C., Gaskell, J., Williams, P.A., Jones, A.C., Chalker, P.R., Marshall, P.A., Smith, L.M., and Critchlow, G.W., *Chem. Vap. Deposition* **10** (2004) 83.

86. Loo, Y.F., Potter, R.J., Jones, A.C., Aspinall, H.C., Gaskell, J., Chalker, P.R., Smith, L.M., and Critchlow, G.W., *Chem. Vap. Deposition* **10** (2004) 306.

87. Aspinall, H.C., Gaskell, J., Loo, Y.F., Jones, A.C., Chalker, P.R., Potter, R.J., Smith, L.M., and Critchlow, G.W., *Chem. Vap. Deposition* **10** (2004) 301.

88. Päiväsaari, J., Niinistö, J., Myllymäki, P., Dezelah, C., Putkonen, M., Nieminen, M., and Niinistö, L., *Topics Appl. Phys.* (2006) In press.

89. Putkonen, M., Nieminen, M., Niinistö, J., Sajavaara, T., and Niinistö, L., *Chem. Mater.* **13** (2001) 4701.

90. Putkonen, M., Sajavaara, T., Johansson, L.-S., and Niinistö, L., *Chem. Vap. Deposition* **7** (2001) 44.

91. Gusev, E.P., Cartier, E., Buchanan, D.A., Gribelyuk, M., Copel, M., Okorn-Schmidt, H., and D'Emic, C., *Microelectron. Eng.* **59** (2001) 341.

92. Mölsä, H., Niinistö, L., and Utriainen, M., *Adv. Mater. Opt. Electron.* **4** (1994) 389.

93. Nieminen, M., Putkonen, M., and Niinistö, L., *Appl. Surf. Sci.* **174** (2001) 155.

94. Mölsä, H. and Niinistö, L., *Mater. Res. Soc. Symp. Proc.* **355** (1994) 341.

95. Niinistö, J., Petrova, N., Putkonen, M., Niinistö, L., Arstila, K., and Sajavaara, T., *J. Cryst. Growth* **285** (2005) 191.

96. Van, T.T. and Chang, J.P., *Appl. Surf. Sci.* **246** (2005) 250.

97. Van, T.T. and Chang, J.P., *Appl. Phys. Lett.* **87** (2005) 011907-1.

98. Van, T.T. and Chang, J.P., *Surf. Sci.* **596** (2005) 1.

99. Potter, R.J., Chalker, P.R., Manning, T.D., Aspinall, H.C., Loo, Y.F., Jones, A.C., Smith, L.M., Critchlow, G.W., and Schumacher, M., *Chem. Vap. Deposition* **11** (2005) 159.

100. Niinistö, J., Putkonen, M., and Niinistö, L., *Chem. Mater.* **16** (2004) 2953.

101. Scarel, G., Bonera, E., Wiemer, C., Tallarida, C., Spiga, S., Fanciulli, M., Fedushkin, I.L., Schumann, H., Lebedenskii, Y., and Zenkevich, A., *Appl. Phys. Lett.* **85** (2004) 630.

102. Gordon, R.G., Becker, J., Hausmann, D., and Suh, S., *Chem. Mater.* **13** (2001) 2463.

103. He, W., Schuetz, S., Solanki, R., Belot, J., and McAndrew, J., *Electrochem. Solid-State Lett.* **7** (2004) G131.

104. Triyoso, D.H., Hegde, R.I., Grant, J., Fejes, P., Liu, R., Roan, D. Ramon, M., Werho, D., Rai, R., La, L.B., Baker, J., Garza, C., Guenther, T., White Jr., B.E., and Tobin, P.J., *J. Vac. Sci. Tech. B* **22** (2004) 2121.

105. Triyoso, D.H., Hegde, R.I., Grant, J., Schaeffer, J.K., Roan, D., White Jr., B.E. and Tobin, P.J., *J. Vac. Sci. Tech. B* **23** (2005) 288.

106. Kukli, K., Ritala, M., Pilvi, T., Sajavaara, T., Leskelä, M., Jones, A.C., Aspinall, H.C., Gilmer, D.C., and Tobin, P.J., *Chem. Mater.* **16** (2004) 5162.

107. Jones, A.C., Aspinall, H.C., Chalker, P.R., Potter, R.J., Kukli, K., Rahtu, A., Ritala, M., and Leskelä, M., *J. Mater. Chem.* **14** (2004) 3101.

108. Kukli, K., Ritala, M., Pore, V., Leskelä, M., Sajavaara, T., Hedge, R.I., Gilmer, D.C., Tobin, P.J., Jones, A.C., and Aspinall, H.C., *Chem. Vap. Deposition* **12** (2006) 158.

109. de Rouffignac, P. and Gordon, R.G., *Abstract Book, AVS 5th International Conference on Atomic Layer Deposition*, San Jose, California, USA, 2005, p. 58.

110. de Rouffignac, P., Park, J.-S., and Gordon, R.G., *Chem. Mater.* **17** (2005) 4808.

111. Lim, B.S, Rahtu, A., Park, J.-S., and Gordon, R.G., *Inorg. Chem.* **42** (2003) 7951.

112. Lim, B.S., Rahtu, A., and Gordon, R.G., *Nature Mater.* **2** (2003) 749.

113. Lim, B.S., Rahtu, A., de Rouffignac, P., and Gordon, R.G., *Appl. Phys. Lett.* **84** (2004) 3957.

114. Binnemans, K., In: *Handbook on the Physics and Chemistry of Rare Earths, Vol. 35* (Eds. K.A. Gschneider Jr, J.-C.G. Bünzli, VK. Pecharsky), Elsevier, Amsterdam 2005, pp. 107-272.

115. Fahlman, B.D. and Barron, A.R., *Adv, Mater. Opt. Electron.* **10** (2000) 223.

116. Tiitta, M. and Niinistö, L., *Chem Vap. Deposition* **3** (1997) 167.

117. Leskelä, M., Niinistö, L., Nykänen, E., Soininen, P., and Tiitta, M., *Thermochim. Acta* **175** (1991) 91.

118. Ozawa, T., *Thermochim. Acta* **174** (1991) 185.

119. Eisentraut, K.J. and Sievers, R.E., *J. Am. Chem. Soc.* **87** (1965) 5254.

120. Leskelä, T., Vasama, K., Härkönen, G., Sarkio, P., and Lounasmaa, M., *Adv. Mater. Opt. Electron.* **6** (1996) 169.

121. Jones, A.C., *J. Mater. Chem.* **12** (2002) 2576.

122. Matero, R., Ritala, M., Leskelä, M., Sajavaara, T., Jones, A.C., and Roberts, J.L., *Chem. Mater.* **16** (2004) 5630.

123. Putkonen, M. and Niinistö, L., *Top. Organomet. Chem.* **9** (2005) 125.

124. Huang, R. and Kitai, A.H., *Appl. Phys. Lett.* **61** (1992) 1450.

125. Lau, J.E., Paterson, G.G., Endisch, D., Barth, K., Topol, A., Kaloyeros, A.E., Tuenge, R.T., and King, C.N., *J. Electrochem. Soc.* **148** (2001) C427.

126. Bradley, D.C., Ghotra, J.S., and Hart, F.A., *J. Chem Soc. Dalton. Trans.* (1973) 1021.

127. Rees Jr., W.S., Just, O., and van Derveer, D.S, *J. Mater. Chem.* **9** (1999) 249.

128. Aspinall, H.C., Williams, P.A., Gaskell, J., Jones, A.C., Roberts, J.L., Smith, L.M., Chalker, P.R., and Critchlow, G.W., *Chem. Vap. Deposition* **9** (2003) 7.

129. Nieminen, M., Sajavaara, T., Rauhala, E., Putkonen, M., and Niinistö, L., *J. Mater. Chem.* **11** (2001) 2340.

130. Seim, H., Mölsä, H., Nieminen, M., Fjellvåg, H., and Niinistö, L., *J. Mater. Chem.* **7** (1997) 449.

131. Seim, H., Nieminen, M., Niinistö, L., Fjellvåg, H., and Johansson, L.-S., *Appl. Surf. Sci*. **112** (1997) 243.

132. Nilsen, O., Peussa, M., Fjellvåg, H., Niinistö, L., and Kjekshus, A., *J. Mater. Chem.* **9** (1999) 1781.

133. Nieminen, M., Lehto, S., and Niinistö, L., *J. Mater. Chem.* 11 (2001) 3148.

134. Nilsen, O., *Growth of Thin Films of Functional Oxides with the ALCVD Method,* Ph.D. Thesis, University of Oslo, Oslo 2003, 33 p.

135. Kosola, A., *Atomic Layer Deposition and Post-deposition Annealing of Perovskite Oxide Thin Films*¸ Licenciate Thesis, Helsinki University of Technology, Helsinki 2005, 75 p.

136. Myllymäki, P., Nieminen, M., Niinistö, J., Putkonen, M., Kukli, K., and Niinistö, L., *J. Mater. Chem.* **16** (2006) 563.

137. Putkonen, M., Sajavaara, T., Niinistö, J., Johansson, L.-S., and Niinistö, L., *J. Mater. Chem.* **12** (2002) 442.

138. Bernay, C., Ringuedé, A., Colomban, P., Lincot, D., and Cassir, M., *J. Phys. Chem. Solids* **64** (2003) 1761.

139. Triyoso, D.H., Li, H., Hedge, R.I., Yu, Z., Moore, K., Grant, J., White Jr, B.E., and Tobin, P.J., *J. Vac. Sci. Technol. B* **23** (2005) 2480.

140. Putkonen, M., Private discussion, 27.3.2006.

141. Sicre, J.E., Dubois, J.T., Eisentraut, K.J., and Sievers, R.E., *J. Am. Chem. Soc.* **91** (1969) 3476.

142. Ha, S.-C., Choi, E., Kim, S.-H., and Roh, J.S., *Thin Solid Films* **476** (2005) 252.

143. Niinistö, J., Putkonen, M., Niinistö, L., Kukli, K., Ritala, M., and Leskelä, M., *J. Appl. Phys.* **95** (2004) 84.

144. Leskelä, M. and Ritala, M., *Angew. Chem.* **42** (2003) 5548.

145. Gusev, E.P., Cabral Jr., C., Copel, M., D'Emic, C., and Gribelyuk, M., *Microelectron. Eng.* **69** (2003) 145.

146. Park, H.B., Cho, M., Park, J., Lee, S.W., Hwang, C.S., Kim, J.-P., Lee, J.-H., Lee, N.-I., Kang, H.-K., Lee, J.-C., and Oh, S.-J., *J. Appl. Phys.* **94** (2003) 3641.

147. Ylilammi, M. and Ranta-aho, T., *Thin Solid Films* **232** (1993) 56.

148. Jokinen, J., Keinonen, J., Tikkanen, P., Kuronen, A., Ahlgren, and Nordlund, K., *Nucl. Instr. Methods B* **119** (1996) 533.

149. Putkonen, M., Sajavaara, T., Niinistö, L., and Keinonen, J., *Anal. Bioanal. Chem.* **382** (2005) 1791.

150. Erasmus, C.D. and Boyens, J.C.A., *Acta Cryst. B* **26** (1970) 1843.

151. Baxter, I., Drake, S.R., Hursthouse, M.B., Abdul Malik, K.M., McAleese, J., Otway, D.J., and Plakatouras, J.C., *Inorg. Chem.* **34** (1995) 1384.

152. Martynenko, L.I., Kuz'mina, N.P., and Grigor'ev, A.N., *Russ. J. Inorg. Chem.* **43** (1998) 1038.

153. De Villiers, J.P.R. and Boyens, J.C.A., *Acta Cryst. B* **28** (1972) 2335.

154. Goldsmith, J.A. and Ross, S.D., *Spectrochim. Acta A* **23** (1967) 1909.

155. Yanagihara, N., Vemulapalli, K., Fernando, Q., and Dyke, J.T., *J. Less-Comm. Met.* **167** (1991) 223.

156. Klingenberg, B. and Vannice, M.A., *Chem. Mater.* **8** (1996) 1755.

157. Leskelä, M. and Niinistö, L., In: *Handbook on the Physics and Chemistry of Rare Earths, Vol. 8*, Elsevier, Amsterdam 1986, pp. 203-334.

158. Kwo, J., Hong, M., Kortan, A.R., Queeney, K.T., Chabal, Y.J., Mannaerts, J.P., Boone, T., Krajewski, J.J., Sergent, A.M., and Rosamilia, J.M., *Appl. Phys. Lett.* **77** (2000) 130.

159. Zhou, J.-P., Chai, C.-L., Yang, S.-Y., Liu, Z.-K., Song, S.-L., Li, Y.-L., and Chen, N.-F., *J. Cryst. Growth* **270** (2004) 21.

160. Song, H.Z., Wang, H.B., Zhang, J., Peng, D.K., and Meng, G.Y., *Mater. Res. Bull.* **37** (2002) 1487.